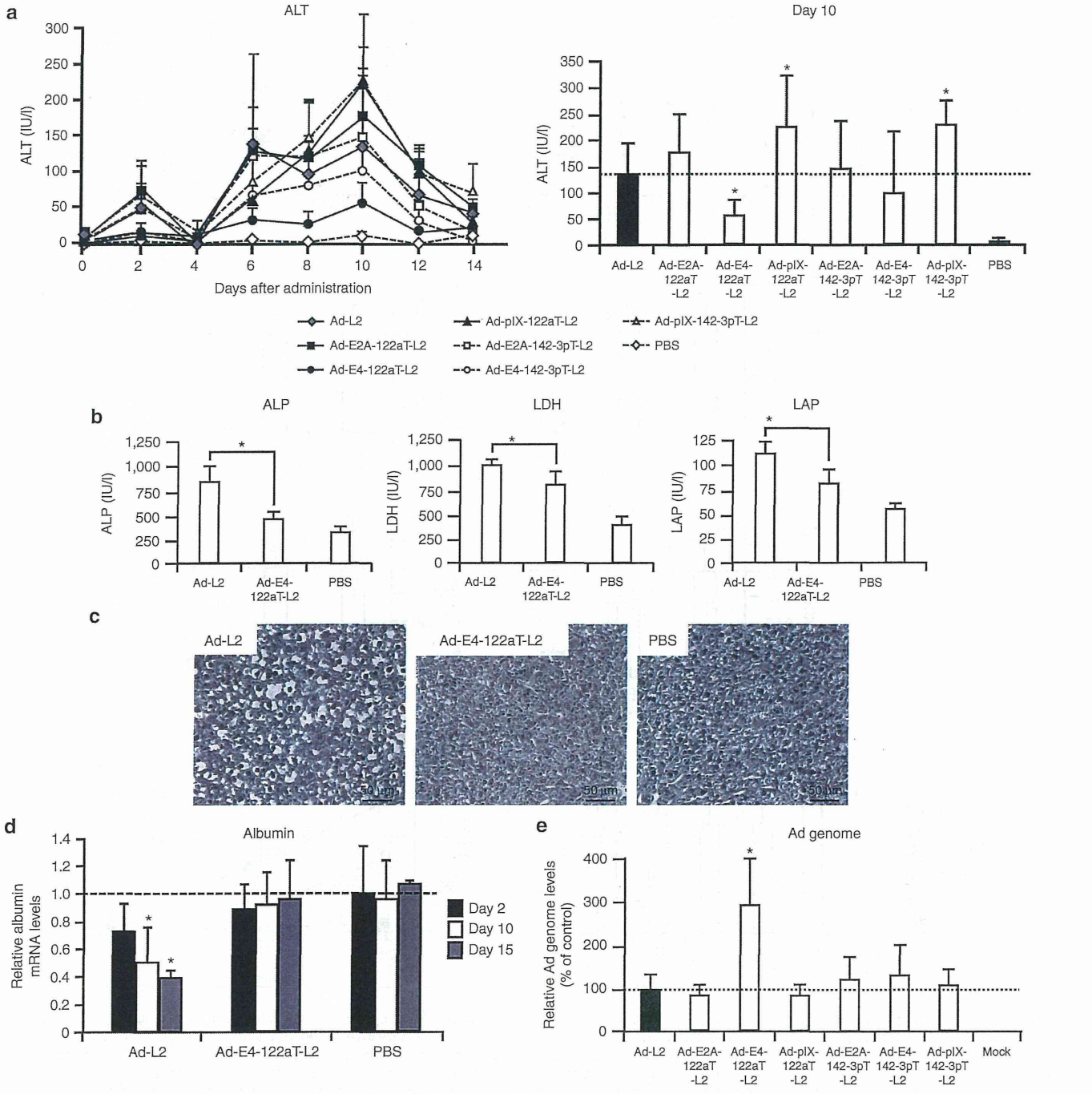

Figure 3 Suppression of Ad vector-mediated hepatotoxicity by incorporation of miR-122a–targeted sequences into the 3′-UTR of the E4 gene. The serum (**a**) ALT, (**b**) ALP, LDH, LAP levels in mice after intravenous injection of Ad vectors. C57BL/6 mice were intravenously administered Ad vectors at 1×10^{10} IFU/mouse. Blood samples were collected *via* retro-orbital bleeding at the indicated number of days after administration. The bar graph shows the serum ALT levels 10 days after administration. The data are expressed as the mean values ± SD ($n = 6$). *$P < 0.05$ in comparison with Ad-L2. Statistically significant differences in the serum ALT levels relative to Ad-L2 were found at 2, 6, 8, 10, 12 days after Ad-E4-122aT-L2 administration. (**c**) Liver sections of mice following intravenous administration of Ad-L2 (left), Ad-E4-122aT-L2 (middle), or PBS (right). C57BL/6 mice were intravenously administered Ad vectors at 1×10^{10} IFU/mouse. Ten days after administration, the livers were isolated, and histological analysis was performed using hematoxylin and eosin staining. The scale bar = 50 μm. (**d**) The albumin mRNA levels in mice after intravenous injection of Ad vectors. C57BL/6 mice were treated with Ad vectors at 1×10^{10} IFU/mouse. The livers were harvested from the mice 2, 10, and 15 days after administration. The data are expressed as the mean values ± SD ($n = 4$–6). *$P < 0.05$ in comparison with PBS. (**e**) Ad genome copy numbers in the liver. C57BL/6 mice were intravenously administered Ad vectors at 1×10^{10} IFU/mouse. Fifteen days after administration, the Ad genome copy numbers in the mouse liver were determined by real-time PCR. The data are expressed as the mean values ± SD ($n = 5$–6). *$P < 0.05$ in comparison with Ad-L2.

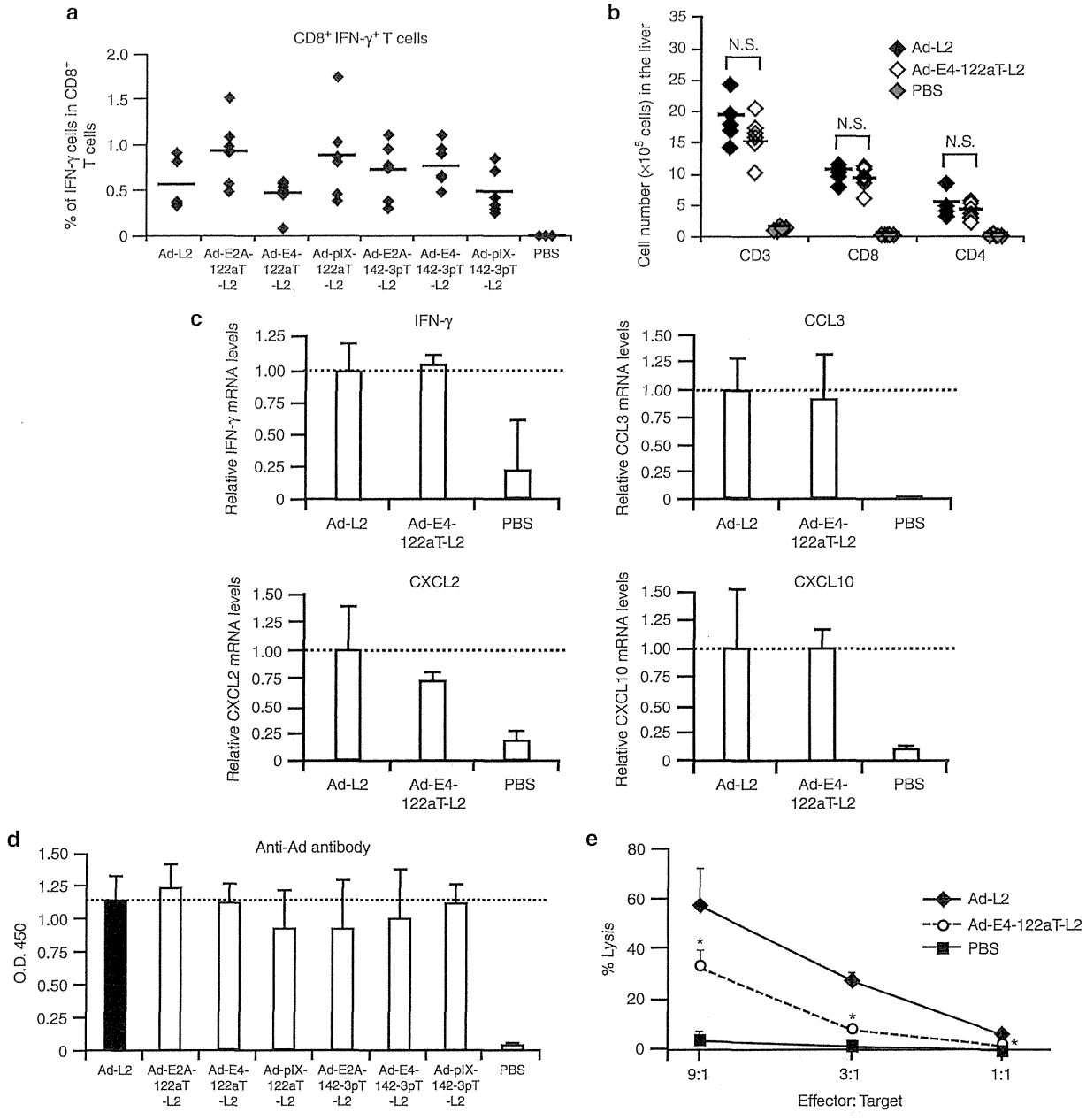

Figure 4 Ad vector-induced immune responses following intravenous administration of Ad vectors into mice. (**a**) Hexon-specific IFN-γ+ CD8+ T cells in the splenocytes. C57BL/6 mice were intravenously administered Ad vectors at 1×10^{10} IFU/mouse. Fifteen days after the injection, the splenocytes were harvested. The splenocytes were incubated with hexon peptide for 6 hours. (**b**) Infiltration of lymphocytes into the liver following Ad vector administration. C57BL/6 mice were intravenously administered Ad vectors at 1×10^{10} IFU/mouse. Ten days after administration, liver mononuclear cells were isolated and analyzed for cells expressing CD3, CD4, and CD8 by fluorocytometry. The data are expressed as the mean values ± SD ($n = 6$). N. S., not significant. (**c**) IFN-γ and chemokine mRNA levels in the liver after administration of Ad-L2 and Ad-E4-122aT-L2. C57BL/6 mice were treated with Ad vectors at 1×10^{10} IFU/mouse. Ten days after administration, IFN-γ and chemokine mRNA levels in the liver were determined by real-time RT-PCR. The data are expressed as the mean values ± SD ($n = 3$–6). (**d**) Anti-Ad antibody levels in the serum following intravenous administration of Ad vectors. C57BL/6 mice were intravenously administered as described above. Anti-Ad antibody levels in the serum were determined by ELISA 14 days after administration. The data are expressed as the mean values ± SD ($n = 6$). (**e**) Ad-specific CTL-mediated lysis of the hepatocytes transduced with Ad vectors. C57BL/6 mice were intravenously administered Ad-null at a dose of 1×10^{10} IFU/mouse. Ten days after the injection, the splenocytes were harvested and incubated with Ad-null at an MOI of 10 for 4 days. Primary mouse hepatocytes were transduced with Ad-L2 or Ad-E4-122aT-L2 at an MOI of 10 for 24 hours and were incubated with the splenocytes at 37 °C. LDH levels in the medium were measured 4 hours after incubation. The data are expressed as the mean values ± SD ($n = 4$). *$P < 0.05$ in comparison with Ad-L2.

DISCUSSION

The aim of this study was to develop a replication-incompetent Ad vector that exhibits an improved safety profile by suppressing the leaky expression of Ad genes, but that can be easily produced at high titers using conventional 293 cells. For this purpose, four tandem copies of sequences with perfect complementarity to miR-122a or miR-142-3p were incorporated into the 3′-UTR of the E2A, E4, or pIX genes. All Ad vectors developed in this study were efficiently produced at high titers comparable to a conventional Ad vector using normal 293 cells. Among the Ad vectors developed, an Ad vector containing the miR-122a–targeted sequences in the 3′-UTR of the E4 gene exhibited lower levels of hepatotoxicity and higher and longer-term transgene expression than a conventional Ad vector. This study also indicates that expression of the E4 gene in the liver is one of the main causes of replication-incompetent Ad vector-induced hepatotoxicity.

Previous studies have developed several types of replication-incompetent Ad vectors lacking the E2A, E4, and/or pIX genes to eliminate the leaky expression of Ad genes and to increase the transgene insertion capacity.[2,10,11] However, the yields of these Ad vectors were frequently much lower than that of a conventional Ad vector. The preparation of HD-Ad vectors also suffers from low yield and a contamination of helper virus.[33] In contrast, the Ad vectors carrying the miRNA-targeted sequences in the 3′-UTR of Ad genes easily grew to high titers comparable to those of a conventional Ad vector *via* a conventional Ad vector preparation method using normal 293 cells without any trouble. High titers of these Ad vectors can be prepared by anyone without much experience in Ad vector preparation. This property is highly crucial not only for studies on potential gene therapies but also for gene function analyses. In particular, an Ad vector with miR-122a–targeted sequences in the 3′-UTR of the E4 gene, which exhibits lower hepatotoxicity and higher and longer-term transgene expression than a conventional Ad vector, would be suitable for gene function analysis in the liver, especially when Ad vector-mediated hepatotoxicity or Ad gene products affect the function of genes of interest. We are currently performing an analysis of gene function in the liver using this Ad vector.

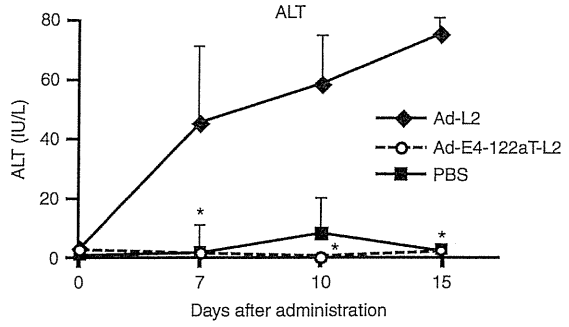

Figure 5 The serum ALT levels in the serum in Rag2/Il2rγ double-knockout mice after intravenous administration of Ad vectors. Rag2/Il2rγ double-knockout mice were intravenously administered Ad vectors at 1×10^{10} IFU/mouse. Blood samples were collected *via* retro-orbital bleeding on the indicated number of days after administration. The data are expressed as the mean values ± SD ($n = 3$). *$P < 0.05$ in comparison with Ad-L2.

Another advantage of an Ad vector containing the miRNA-targeted sequences in the 3′-UTR of the E4 gene is that the expression of all E4 ORFs is suppressed by miRNA. The miRNA-targeted sequences were inserted into the common terminal sequence, which is shared by all E4 ORFs, in the 3′-UTR.[21] We confirmed that all E4 ORF mRNAs possessed the miRNA-targeted sequences in the 3′-UTR without mutations. In addition, all of the RT-PCR products of E4 gene transcripts by 4 different pairs of primers, each of which can detect several different E4 ORFs, were reduced, indicating that all of the E4 ORF mRNA levels were reduced by insertion of the miRNA-targeted sequences in the common terminal sequence in the 3′-UTR (data not shown). It is highly difficult to produce high titers of an Ad vector in which the E4 ORFs are completely deleted. There have been only two studies demonstrating the *in vivo* transduction properties of Ad vectors with deletion of all E4 ORFs,[8,34] although various types of Ad vectors containing mutations in the E4 gene have been developed.[2,3,10] As described below, the E4 gene products have inhibitory effects on various cellular functions, suggesting that

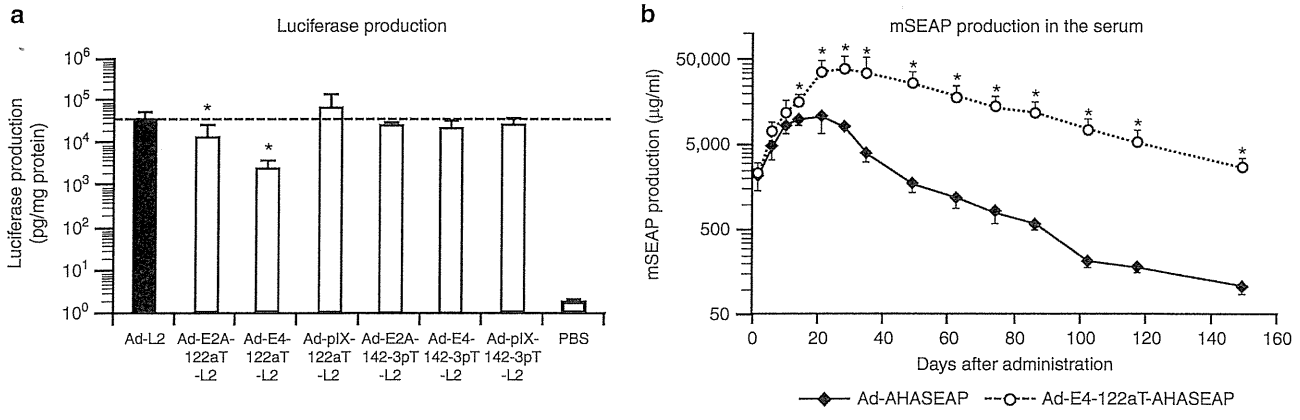

Figure 6 Ad vector-mediated transgene expression in mice. (**a**) Luciferase production in the liver following Ad vector administration. C57BL/6 mice were intravenously administered Ad vectors expressing the luciferase gene under the control of a CMV promoter at 1×10^{10} IFU/mouse, and the livers were harvested and subjected to luciferase expression analysis 2 days after administration. Luciferase production in the liver was determined by luminescence assay. The data are expressed as the mean values ± SD ($n = 5$–6). *$P < 0.05$ in comparison with Ad-L2. (**b**) mSEAP production in the serum following Ad vector administration. C57BL/6 mice were intravenously administered Ad vectors expressing the mSEAP gene under the control of an AHA promoter at 1×10^{10} IFU/mouse. Blood samples were collected *via* retro-orbital bleeding on the indicated days after injection. mSEAP production in the serum was determined by SEAP chemiluminescence assay. The data are expressed as the mean values ± SD ($n = 4$). *$P < 0.05$ in comparison with Ad-AHASEAP. mSEAP expression in the PBS-treated mice was below the detectable level.

the suppression of all E4 ORF expression is crucial in order to reduce Ad vector-mediated hepatotoxicity.

In addition to the E4 gene-deleted Ad vectors, the E2A gene-deleted Ad vectors were developed and exhibited the reduction in expression of not only the E2A gene but also Ad late genes in the cultured cells.[4] In this study, insertion of the miR-122a–targeted sequences in the 3′-UTR of the E2A gene resulted in a 2-log order reduction in the expression of the E2A gene in the liver, compared with Ad-L2. Ad-E2A-122aT-L2 also exhibited a 2-log order reduction in the expression of the Ad late genes in the liver because the E2A gene product is essential for viral genome replication;[4] however, serum ALT levels following administration of Ad-E2A-122aT-L2 were comparable to those by Ad-L2 and higher than those by Ad-E4-122aT-L2. These results suggest that the E4 gene expression in the liver plays a crucial role in Ad vector-induced hepatotoxicity. Christ *et al.* also demonstrated that deletion of the E4 gene resulted in much greater suppression of the hepatotoxicity than deletion of the E2A gene.[4]

miR-122a, which is a liver-specific miRNA, is a very effective choice of miRNA for the regulation of the Ad vector-mediated expression of both the transgene and Ad genes, because Ad vectors have strong hepatotropism. In addition, a very high copy number of miR-122a is expressed in the liver hepatocytes. miR-122a accounts for approximately 70% of the miRNAs expressed in the hepatocytes.[20] We previously reported that Ad vector-mediated transgene expression in the liver and replication of oncolytic adenoviruses containing a tumor-specific promoter in the hepatocytes were efficiently suppressed by insertion of miR-122a–targeted sequences into the 3′-UTR of transgene.[15,16] Ylösmaki *et al.* reported that the insertion of miR-122a–targeted sequences into the E1A gene in replication-competent Ad reduced hepatotoxicity.[35]

At the beginning of this study, we hypothesized that leaky expression in the spleen, which is considered to play a crucial role in induction of CTLs, should be suppressed in order to suppress the induction of Ad protein-specific CTLs, and that the insertion of miR-142-3p–targeted sequences into the 3′-UTR of Ad genes would reduce the leaky expression of Ad genes in the spleen. However, the leaky expression levels of Ad genes in the spleen were 50- to 5,000-fold lower than those in the liver following intravenous administration of Ad-L2. In particular, the expression levels of the Ad late genes by all Ad vectors in the spleen were extremely low and slightly above the detection limit of real-time RT-PCR analysis. Hexon-specific CTL induction was not suppressed by miRNA-mediated inhibition of Ad gene expression in the spleen, although all the Ad vectors except for Ad-E2A-142-3pT-L2 and Ad-pIX-142-3pT-L2 exhibited significantly lower leaky expression levels of Ad genes in the spleen, compared with Ad-L2. In addition, the numbers of lymphocytes infused into the liver and IFN-γ mRNA levels in the liver were comparable between mice receiving Ad-L2 and those treated with Ad-E4-122aT-L2. These results suggest that Ad protein-specific CTLs might be mainly induced by Ad input proteins taken up by spleen antigen-presenting cells. Several studies have demonstrated the contribution of Ad input proteins to Ad protein-specific CTL responses.[36,37] Significant levels of CTLs were detected by HD-Ad vectors and UV-inactivated Ad vectors following intravenous administration into mice.[36,38] A previous study reported a significant reduction in the CTL levels following administration of an Ad vector with deletion of the E2A or E4 gene;[2] however, a CTL against the transgene product might have been measured in that study. Although Ad vector-mediated CTL induction in the spleen and infiltration of lymphocytes in the liver were comparable between Ad-L2 and Ad-E4-122aT-L2, the CTL-mediated damages in the hepatocytes transduced with Ad-E4-122aT-L2 were significantly lower than those in the cells treated with Ad-L2. This is probably because the leaky expression of Ad genes in the liver was greatly reduced in the case of Ad-E4-122aT-L2 transduction, leading to a reduction in Ad antigen presentation on the hepatocytes.

This study demonstrated that miR-122a–mediated suppression of the E4 gene expression in the liver significantly reduced the hepatotoxicity that was caused by a replication-incompetent Ad vector *via* not only an adaptive immune response but also a non-adaptive immune response, indicating that the E4 gene products expressed in the liver directly induced hepatotoxicity *via* a non-adaptive immune response. Several studies have also reported that E4 gene products caused hepatotoxicity even in immune-incompetent mice following systemic administration.[2,39] The E4 gene products have various functions. For example, the E4 ORF3 and E4 ORF6 augment viral DNA replication, late viral protein synthesis, and shut-off of host protein synthesis, and the E4 ORF4 has been demonstrated to be involved in apoptosis.[21,25] However, the detailed mechanism of the E4 gene product-mediated hepatotoxicity following Ad vectors administration remains to be elucidated. Christ *et al.* prepared a series of Ad vectors containing various combinations of the E4 ORFs, and examined the hepatotoxicity profiles of these Ad vectors. They demonstrated that liver injury was markedly reduced with vectors containing either the E4 ORF3 alone or the ORF3+ ORF4, while vectors containing the ORF4 alone, the ORF6+ ORF6/7, or ORF3+ ORF6+ ORF6/7 still displayed elevated hepatotoxicity.[9] Other groups also reported the hepatotoxicity profiles of the Ad vectors containing various patterns of deletion in the E4 genes.[2,10] Taken together, these results indicate that the mechanism of the E4 ORF-induced hepatotoxicity is highly complex, and it has remained unclear which E4 ORF is crucial for Ad vector-mediated hepatotoxicity. Therefore, suppression of the expression of all E4 gene products from the Ad vector genome is crucial to suppress the Ad vector-mediated hepatotoxicity, as described above.

In summary, replication-incompetent Ad vectors exhibiting miRNA-mediated suppression of the leaky expression of Ad genes were developed in this study. All Ad vectors developed were easily produced at high titers comparable to a conventional Ad vector using normal 293 cells. Among the Ad vectors developed, an Ad vector containing miR-122a–targeted sequences into the 3′-UTR of the E4 gene exhibited lower levels of liver damage and higher transgene expression profiles, compared with a conventional Ad vector. Furthermore, this study indicates that expression of the E4 gene in the liver is one of the main causes of Ad vector-induced hepatotoxicity. An Ad vector with miR-122a–targeted sequences in the 3′-UTR of the E4 genes would be a promising framework for safe and effective gene therapy, basic research including gene function analysis, and elucidation of the mechanisms underlying Ad vector-mediated toxicity.

MATERIALS AND METHODS

Mice and cells

Female C57BL/6 mice aged 5–7 weeks were obtained from Nippon SLC (Hamamatsu, Japan). Rag2/Il2rγ double-knockout mice of a C57BL/6 background, also aged 5–7 weeks, were obtained from Taconic Farms (Hudson, NY).[31] All animal experimental procedures used in this study were performed in accordance with the institutional guidelines for animal experiments at Osaka University. HuH-7 cells (a human well-differentiated hepatocellular carcinoma cell line) were cultured in Dulbecco's modified Eagle's medium (Sigma-Aldrich, St Louis, MO) supplemented with 10% fetal calf serum (FCS) and antibiotics. A total of 293 cells (a human embryonic kidney cell line) were cultured in Dulbecco's modified Eagle's medium (Wako Pure Chemical Industries, Osaka, Japan) supplemented with 10% FCS, 2 mmol/l glutamine (Wako Pure Chemical Industries), and antibiotics. Primary mouse hepatocytes

were cultured in Williams' Medium E (Life Technologies, Carlsbad, CA) supplemented with 10% FCS, 10 μg/ml insulin (Sigma-Aldrich), 4 μg/ml dexamethasone (Wako Pure Chemical Industries), and antibiotics.

Plasmid and replication-incompetent Ad vectors

Ad vector plasmids containing miRNA-targeted sequences were constructed as follows. Briefly, for construction of the plasmid for an Ad vector incorporating miRNA-targeted sequences into the 3′-UTR of the E2A gene, the Ad genome fragment (bp 21562-25204) was cloned into the *BamH*I/*Sac*I sites in pHM5.[40] Subsequently, the *Bst*XI site was introduced into the *Dra*I site (bp 22444) in the 3′-UTR of the E2A gene by ligation with the oligonucleotides encoding the *Bst*XI site (E2A-3′-UTR-F and E2A-3′-UTR-R; Supplementary Table S1). Following the introduction of oligonucleotides encoding two copies of miR-122a complementary sequences and *Pac*I/*Spe*I sites (E2A-miR-122aT-BstXI-S3 and E2A-miR-122aT-BstXI-AS3) into the *Bst*XI site, oligonucleotides encoding two copies of miR-122a complementary sequences (E2A-miR-122aT-BstXI-S4 and E2A-miR-122aT-BstXI-AS4) were introduced into the *Pac*I/*Spe*I sites. The fragment containing the miRNA-targeted sequences was replaced with the corresponding sequences in the conventional Ad vector genome in pAdHM4[40] by homologous recombination, resulting in pAdHM4-E2A-122aT. For construction of the plasmid for an Ad vector incorporating miRNA-targeted sequences into the 3′-UTR of the E4 gene, the Ad genome fragment (bp 31993-33283) was cloned into pHM3.3, which was constructed based on pHM3.[40] Subsequently, the *Kpn*I site was introduced into the *Apo*I/*BspM*I sites (bp 32835-35943), which were located in the 3′-UTR of the E4 gene, by ligation with oligonucleotides encoding the *Kpn*I site (E4-3′-UTR-F1 and E4-3′-UTR-R1). Thereafter, the *Not*I site was introduced into the *Kpn*I/*BspM*I sites (bp 32943), which were located in the 3′-UTR of the E4 gene, by ligation with oligonucleotides encoding the *Not*I site (E4-3′-UTR-F2 and E4-3′-UTR-R2). Following the introduction of oligonucleotides encoding two copies of miR-122a complementary sequences and the *Pac*I site (E4-miR-122aT-S1 and E4-miR-122aT-AS1) into the *Kpn*I/*Not*I sites, oligonucleotides encoding two copies of miR-122a complementary sequences (E4-miR-122aT-S2 and E4-miR-122aT-AS2) were introduced into the *Kpn*I/*Pac*I sites. The fragment containing the miRNA-targeted sequences was replaced with the conventional Ad vector genome in pAdHM4 by homologous recombination, resulting in pAdHM4-E2A-122aT. For construction of a plasmid for an Ad vector incorporating miRNA-targeted sequences into the 3′-UTR of the pIX gene, the *Kpn*I and *EcoR*I sites were introduced into the *Xba*I site (bp 4030), which is located in the 3′-UTR of the pIX gene, in pAd3′-IX5, which was constructed based on pAdHM41.[41] Oligonucleotides encoding the miR-122a–targeted sequences (pIX-miR-122aT-S1, pIX-miR-122aT-AS1, pIX-miR-122aT-S2, and pIX-miR-122aT-AS2) were inserted into the *Kpn*I and *EcoR*I sites. The resulting plasmid was then digested with PI-*Sce*I/*BstZ*17I, and ligated with PI-*Sce*I/*BstZ*171-digested pAdHM4, resulting in pAdHM4-pIX-122aT. The sequences of the oligonucleotides are shown in Supplementary Table S1. Ad vector plasmids incorporating four tandem copies that were perfectly complementary to miR-142-3p were similarly constructed using the oligonucleotides encoding miR-142-3p–targeted sequences (Supplementary Table S1). The sequences of the miRNA-targeted sequences in the Ad vector plasmids were verified by sequence analysis.

Ad vectors were prepared by an improved *in vitro* ligation method.[40,42] An AHA-driven mSEAP-expressing plasmid, pAHA-mSEAP, was constructed using pHMRSV6,[42] pBS-ApoEHCR-hAATp-hFIX-Int-bpA,[43] and pCpG-mSEAP (InvivoGen, SanDiego, CA). pCMVL1,[22] which has a CMV promoter-driven luciferase expression cassette, and pAHA-mSEAP were digested with I-*Ceu*I/PI-*Sce*I, and subsequently ligated with I-*Ceu*I/PI-*Sce*I–digested Ad vector plasmids. Further details on the construction method of Ad vector plasmids are available upon request. Each Ad vector plasmid was digested with *Pac*I to release the recombinant viral genome, and was transfected into conventional 293 cells plated on 60-mm dishes. All Ad vectors were propagated in 293 cells, purified by two rounds of cesium chloride-gradient ultracentrifugation, dialyzed, and stored at −80 °C. The virus particles (VPs) were determined using a spectrophotometric method,[44] and biological titers were measured using an Adeno-X-rapid titer kit (Clontech, Mountain View, CA). The ratio of the particle-to-biological titer was between 6.5 and 8 for each Ad vector used in this study. We confirmed by PCR analysis that none of the viral stocks used in this study contained detectable replication-competent virus.[45] The Ad vectors used in this study are listed in Table 1.

In vitro Ad gene expression analysis

HuH-7 cells were seeded into 12-well plates at 1×10^5 cells/well. On the following day, cells were transduced with Ad vectors at a multiplicity of infection (MOI) of 10 for 1 hour. The medium containing Ad vectors was replaced with fresh medium after a 1-hour incubation. HuH-7 cells were harvested 12 hours after transduction, and total RNA was extracted from the cells. The mRNA levels of Ad genes and the glyceroaldehyde-3-phosphate-dehydrogenase (GAPDH) gene were evaluated by real-time PCR analysis as previously described.[46] In the inhibition experiments using LNA-modified ASO complementary to miR-122a (miRCURY LNA Power Inhibitor; Exiqon, Vedbaek, Denmark) or an LNA control,[47] HuH-7 cells were transfected with the ASO at 10 nmol/l using Lipofectamine2000 (Invitrogen, Carlsbad, CA). Twenty-four hours after transfection, HuH-7 cells were transduced with Ad vectors at MOIs of 10 for 1 hour, and harvested 12 hours after transduction. After total RNA isolation, mRNA levels of Ad genes were determined by real-time RT-PCR as described above.

In vivo Ad gene expression analysis

Ad vectors were intravenously administered into C57BL/6 mice at a dose of 1×10^{10} IFU/mouse *via* the tail vein. Total RNA was extracted from the livers and spleens at the indicated number of days following administration. The Ad gene mRNA levels in the organs were determined as previously described.[46] The sequences of the primers and probe of mouse GAPDH were as follows: forward, 5′-CAA TGT GTC CGT CGT GGA TCT-3′; reverse, 5′-GTC CTC AGT GTA GCC CAA GAT G-3′; probe, FAM-CGT GCC GCC TGG AGA AAC CTG CC-TAMRA.

Analysis of Ad vector-mediated hepatotoxicity following intravenous administration

Ad vectors were intravenously administered into C57BL/6 and Rag2/Il2rγ double-knockout mice at a dose of 1×10^{10} IFU/mouse. The blood samples were collected *via* retro-orbital bleeding at the indicated days, and the serum samples were obtained by centrifugation. The serum ALT levels were determined using a transaminase-CII kit (Wako Pure Chemical Industries). The serum levels of ALP, LDH, and LAP were analyzed at the Oriental Yeast Corporation (Tokyo, Japan). For the histopathological examination of liver sections, the livers were recovered from C57BL/6 mice 10 days following Ad vector administration. The livers were washed, fixed in 10% buffered formalin (Wako Pure Chemical Industries), embedded in paraffin, and processed for histology.

Albumin mRNA levels in the liver following Ad vector administration were determined by real-time RT-PCR using THUNDERBIRD SYBR qPCR Mix (TOYOBO, Osaka, Japan). The protocol for thermal cycling consisted of 60 seconds at 95 °C, followed by 40 cycles of 15 seconds at 95 °C and 60 seconds at 60 °C. The sequences of the primers were as follows: forward, 5′-TCC AAA CCT CCG TGA AAA CTA TG-3′; reverse, 5′-TGT GTT GCA GGA AAC ATT CGT-3′.

Analysis of Ad vector genome copy numbers in the liver

Ad vectors were intravenously administered into C57BL/6 mice at a dose of 1×10^{10} IFU/mouse, and liver homogenates were prepared as described above at 15 days after administration. Total DNA, including Ad vector genome, was extracted from the liver homogenates. Ad genome copy numbers in the liver were examined similarly as Ad gene expression analysis.

Analysis of Ad hexon-specific CTLs by intracellular cytokine staining assay

Levels of Ad hexon-specific CTLs in the spleen were evaluated 15 days after administration of Ad vectors at 1×10^{10} IFU/mouse using a Cytofix/CytoPerm Plus kit (BD Biosciences, San Diego, CA) as previously described with slight modification.[48,49] Briefly, the spleen was harvested from the mice 15 days after administration, and 2×10^6 splenocytes were incubated for 6 hours with Ad hexon peptide (Milteny Biotec, Bergisch Gladbach, Germany), costimulatory antibodies (Ab) (CD28 and CD49d, 37.51 and R1-2,1 μg/ml; eBioscience, San Diego, CA), and 1 μg/ml of GolgiStop (BD Biosciences) in the RPMI1640 (Sigma-Aldrich) medium at 37 °C. After the incubation, the cells were washed with PBS and stained for viability (Live/Dead Fixable Dead Cell Stain Kits; Invitrogen) for 30 minutes at room temperature. The cells were then washed and stained with phycoerythrin (PE)-Cy7-conjugated anti-mouse CD3ε Ab (145-2C; eBioscience) and allophycocyanin (APC)-Cy7-conjugated anti-mouse CD8 Ab (53-6.7; BioLegend, San Diego, CA) for 30 minutes at 4 °C. Following incubation and washing with PBS, the cells were incubated with Cytofix/Cytoperm solution for

25 minutes at 4 °C for permeabilization, and stained with PE-conjugated anti-mouse interferon (IFN)-γ Ab (XMG1.2; eBioscience) after washing with Perm/Wash solution (BD Biosciences). Data were analyzed using FlowJo software (TreeStar, Ashland, OR).

Evaluation of intrahepatic lymphocytes following Ad vector administration

Intrahepatic lymphocytes were recovered from the livers of Ad vector-treated C57BL/6 mice 10 days after administration as follows. The livers were perfused *via* the portal vein with PBS, cut, and homogenized using a plunger. The liver cell suspension was passed through a mesh in PBS containing 5 mg/ml collagenase and 100 U/ml DNaseI (Roche, Basel, Switzerland). The cell suspension was incubated for 45 minutes at 37 °C and centrifuged at 300*g* for 6 minutes at 4 °C. The cell pellet was then resuspended in serum-free RPMI1640 medium containing 44% Percoll, added to PBS containing 55% Percoll, and centrifuged at 300*g* for 20 minutes at room temperature. The cell fraction was harvested, added to 2% FCS-PBS, centrifuged at 300*g*, washed with 2% FCS-PBS, and resuspended in 1 ml of red blood cell lysis solution (1×Ack buffer) for 1 minutes at 4 °C. Cells were then washed twice and resuspended in 2% FCS-PBS. For fluorescence activated cell sorting (FACS) analysis, total mononuclear cells were stained for viability with fluorescein isotiocyanate (FITC)-conjugated anti-mouse CD4 Ab (GK1.5, eBioscience), anti-mouse CD3ε Ab, and anti-mouse CD8 Ab, and subsequently subjected to FACS analysis. Data were analyzed using FlowJo software (TreeStar).

Expression of IFN-γ and chemokines in the liver after Ad vector administration

The Ad vectors were intravenously administered to C57BL/6 mice at a dose of 1×10^{10} IFU/mouse. Ten days after administration, total RNA was extracted from the livers. The IFN-γ and chemokine production levels were determined by real-time RT-PCR using THUNDERBIRD SYBR qPCR Mix (TOYOBO, Osaka, Japan) as described above. The sequences of the primers used in this study are listed in Supplementary Table S2.

CTL-mediated lysis of Ad vector-transduced primary mouse hepatocytes

A C57BL/6 mouse was intravenously administered Ad-null,[40] which does not possess a transgene expression cassette, at 1×10^{10} IFU/mouse to induce Ad-specific CTL. The spleen was harvested from the mouse 10 days after administration, and splenocytes were restimulated with Ad-null at an MOI of 10 for 4 days. Primary hepatocytes were isolated from a naive mouse using the hepatic portal perfusion technique *via* a conventional method.[50] Primary hepatocytes were seeded into a 96-well round bottom plate at 1×10^4 cells/well. One day after isolation, primary hepatocytes were transduced with Ad-L2 or Ad-E4-122aT-L2 at an MOI of 10. The medium containing Ad vectors was replaced with fresh medium after a 24-hour incubation. Subsequently, the primary hepatocytes were incubated with the splenocytes isolated as described above for 4 hours at 37 °C. The CTL-mediated lysis was measured by an LDH assay using a CytoTox 96 Non-Radioactive Cytotoxicity Assay (Promega, Madison, WI) as previously described.[38,51]

Anti-Ad antibody levels in the serum following intravenous administration of Ad vectors

C57BL/6 mice were intravenously administered Ad vectors at 1×10^{10} IFU/mouse. Blood samples were collected *via* retro-orbital bleeding fourteen days after administration. Anti-Ad antibody levels in the serum were determined by enzyme-linked immunosorbent assay (ELISA). For the ELISA, a 96-well plate was coated with Ad-null (5×10^5 IFU/well) overnight at 4 °C, washed with PBS-0.05% Tween (PBST), and blocked in ImmunoBlock (DS Pharma Biomedical, Osaka, Japan) for 1 hour at room temperature. The serum samples (diluted 1:500) were added to the antigen-coated plate and incubated for 2 hours at 37 °C. The plate was washed with PBST and incubated with biotin-conjugated goat anti-mouse IgG (H+L) (SouthernBiotech, Birmingham, AL) for 2 hours at 37 °C. The plates was then washed with PBST and incubated with streptavidin-HRP (SouthernBiotech) for 1 hour at room temperature. Finally, the plate was washed with PBST and TMB ELISA Peroxidase Substrate (Rockland Immunochemicals, Gilbertsville, PA) was added. The reaction was stopped by the addition of 0.5 mol/l HCl, and absorbance was read at 450 nm on a TriStar LB941 (Berthold Technologies, Bad Wildbad, Germany).

In vivo transgene expression analysis

Ad vectors were intravenously administered into C57BL/6 mice at a dose of 1×10^{10} IFU/mouse. Two days after administration, the livers were recovered from the mice and homogenized. The luciferase production in the homogenates was measured as previously described.[52] For determination of mSEAP levels in the serum, C57BL/6 mice were administered the Ad vectors expressing mSEAP at a dose of 1×10^{10} IFU/mouse. The blood samples were collected on the indicated days *via* retro-orbital bleeding. mSEAP expression levels were determined using Great EscAPe SEAP Chemiluminescence Kit, version 2.0 (Clontech).

Statistical analysis

Statistical significance ($P < 0.05$) was determined using Student's *t*-test. Data are presented as means ± SD.

CONFLICT OF INTEREST

The authors declare no conflict of interest.

ACKNOWLEDGMENTS

The authors thank Kazuo Ohashi (Graduate School of Pharmaceutical Sciences, Osaka University, Osaka, Japan), Takako Ichinose (National Institute of Biomedical Innovation, Osaka, Japan), and Sayuri Okamoto (Graduate School of Pharmaceutical Sciences, Osaka University, Osaka, Japan) for their help, and David R Corey (University of Texas, Southwestern Medical Center, Dallas, TX) for advice. The AHA promoter was kindly provided by Mark A Kay (Stanford University, CA). This work was supported by a grant-in-aid for Young Scientists (A) and a Grant-in-Aid for Scientific Research (A) and (B) from the Ministry of Education, Culture, Sports, Sciences, and Technology (MEXT) of Japan, by a grant from the Ministry of Health, Labour and Welfare of Japan, and a grant from the Japan Research Foundation for Clinical Pharmacology. K.S., K.T., and Y.N. are research fellows of the Japan Society for the Promotion of Science.

REFERENCES

1. Yang, Y, Nunes, FA, Berencsi, K, Furth, EE, Gönczöl, E and Wilson, JM (1994). Cellular immunity to viral antigens limits E1-deleted adenoviruses for gene therapy. *Proc Natl Acad Sci USA* **91**: 4407–4411.
2. Gao, GP, Yang, Y and Wilson, JM (1996). Biology of adenovirus vectors with E1 and E4 deletions for liver-directed gene therapy. *J Virol* **70**: 8934–8943.
3. Dedieu, JF, Vigne, E, Torrent, C, Jullien, C, Mahfouz, I, Caillaud, JM *et al.* (1997). Long-term gene delivery into the livers of immunocompetent mice with E1/E4-defective adenoviruses. *J Virol* **71**: 4626–4637.
4. Lusky, M, Christ, M, Rittner, K, Dieterle, A, Dreyer, D, Mourot, B *et al.* (1998). *In vitro* and *in vivo* biology of recombinant adenovirus vectors with E1, E1/E2A, or E1/E4 deleted. *J Virol* **72**: 2022–2032.
5. Schaack, J, Qiao, L, Walkiewicz, MP, Stonehouse, M, Engel, DA, Vazquez-Torres, A *et al.* (2011). Insertion of CTCF-binding sites into a first-generation adenovirus vector reduces the innate inflammatory response and prolongs transgene expression. *Virology* **412**: 136–145.
6. Nakai, M, Komiya, K, Murata, M, Kimura, T, Kanaoka, M, Kanegae, Y *et al.* (2007). Expression of pIX gene induced by transgene promoter: possible cause of host immune response in first-generation adenoviral vectors. *Hum Gene Ther* **18**: 925–936.
7. Zhou, H, O'Neal, W, Morral, N and Beaudet, AL (1996). Development of a complementing cell line and a system for construction of adenovirus vectors with E1 and E2a deleted. *J Virol* **70**: 7030–7038.
8. Brough, DE, Hsu, C, Kulesa, VA, Lee, GM, Cantolupo, LJ, Lizonova, A *et al.* (1997). Activation of transgene expression by early region 4 is responsible for a high level of persistent transgene expression from adenovirus vectors in vivo. *J Virol* **71**: 9206–9213.
9. Christ, M, Louis, B, Stoeckel, F, Dieterle, A, Grave, L, Dreyer, D *et al.* (2000). Modulation of the inflammatory properties and hepatotoxicity of recombinant adenovirus vectors by the viral E4 gene products. *Hum Gene Ther* **11**: 415–427.
10. Andrews, JL, Kadan, MJ, Gorziglia, MI, Kaleko, M and Connelly, S (2001). Generation and characterization of E1/E2a/E3/E4-deficient adenoviral vectors encoding human factor VIII. *Mol Ther* **3**: 329–336.
11. Krougliak, V and Graham, FL (1995). Development of cell lines capable of complementing E1, E4, and protein IX defective adenovirus type 5 mutants. *Hum Gene Ther* **6**: 1575–1586.
12. Mian, A, Guenther, M, Finegold, M, Ng, P, Rodgers, J and Lee, B (2005). Toxicity and adaptive immune response to intracellular transgenes delivered by helper-dependent vs. first generation adenoviral vectors. *Mol Genet Metab* **84**: 278–288.
13. Reddy, PS, Sakhuja, K, Ganesh, S, Yang, L, Kayda, D, Brann, T *et al.* (2002). Sustained human factor VIII expression in hemophilia A mice following systemic delivery of a gutless adenoviral vector. *Mol Ther* **5**: 63–73.

14. Brown, BD, Venneri, MA, Zingale, A, Sergi Sergi, L and Naldini, L (2006). Endogenous microRNA regulation suppresses transgene expression in hematopoietic lineages and enables stable gene transfer. *Nat Med* **12**: 585–591.
15. Suzuki, T, Sakurai, F, Nakamura, S, Kouyama, E, Kawabata, K, Kondoh, M *et al.* (2008). miR-122a-regulated expression of a suicide gene prevents hepatotoxicity without altering antitumor effects in suicide gene therapy. *Mol Ther* **16**: 1719–1726.
16. Bennett, D, Sakurai, F, Shimizu, K, Matsui, H, Tomita, K, Suzuki, T *et al.* (2012). Further reduction in adenovirus vector-mediated liver transduction without largely affecting transgene expression in target organ by exploiting microrna-mediated regulation and the Cre-loxP recombination system. *Mol Pharm* **9**: 3452–3463.
17. Kron, MW, Espenlaub, S, Engler, T, Schirmbeck, R, Kochanek, S and Kreppel, F (2011). miRNA-mediated silencing in hepatocytes can increase adaptive immune responses to adenovirus vector-delivered transgenic antigens. *Mol Ther* **19**: 1547–1557.
18. Sugio, K, Sakurai, F, Katayama, K, Tashiro, K, Matsui, H, Kawabata, K *et al.* (2011). Enhanced safety profiles of the telomerase-specific replication-competent adenovirus by incorporation of normal cell-specific microRNA-targeted sequences. *Clin Cancer Res* **17**: 2807–2818.
19. Kelly, EJ and Russell, SJ (2009). MicroRNAs and the regulation of vector tropism. *Mol Ther* **17**: 409–416.
20. Lagos-Quintana, M, Rauhut, R, Yalcin, A, Meyer, J, Lendeckel, W and Tuschl, T (2002). Identification of tissue-specific microRNAs from mouse. *Curr Biol* **12**: 735–739.
21. Täuber, B and Dobner, T (2001). Molecular regulation and biological function of adenovirus early genes: the E4 ORFs. *Gene* **278**: 1–23.
22. Mizuguchi, H, Koizumi, N, Hosono, T, Utoguchi, N, Watanabe, Y, Kay, MA *et al.* (2001). A simplified system for constructing recombinant adenoviral vectors containing heterologous peptides in the HI loop of their fiber knob. *Gene Ther* **8**: 730–735.
23. Cawood, R, Chen, HH, Carroll, F, Bazan-Peregrino, M, van Rooijen, N and Seymour, LW (2009). Use of tissue-specific microRNA to control pathology of wild-type adenovirus without attenuation of its ability to kill cancer cells. *PLoS Pathog* **5**: e1000440.
24. Merkerova, M, Belickova, M and Bruchova, H (2008). Differential expression of microRNAs in hematopoietic cell lineages. *Eur J Haematol* **81**: 304–310.
25. Weitzman, MD (2005). Functions of the adenovirus E4 proteins and their impact on viral vectors. *Front Biosci* **10**: 1106–1117.
26. Wilusz, CJ, Wormington, M and Peltz, SW (2001). The cap-to-tail guide to mRNA turnover. *Nat Rev Mol Cell Biol* **2**: 237–246.
27. Gallo-Penn, AM, Shirley, PS, Andrews, JL, Tinlin, S, Webster, S, Cameron, C *et al.* (2001). Systemic delivery of an adenoviral vector encoding canine factor VIII results in short-term phenotypic correction, inhibitor development, and biphasic liver toxicity in hemophilia A dogs. *Blood* **97**: 107–113.
28. Parks, RJ (2005). Adenovirus protein IX: a new look at an old protein. *Mol Ther* **11**: 19–25.
29. Molinier-Frenkel, V, Lengagne, R, Gaden, F, Hong, SS, Choppin, J, Gahery-Ségard, H *et al.* (2002). Adenovirus hexon protein is a potent adjuvant for activation of a cellular immune response. *J Virol* **76**: 127–135.
30. Shinkai, Y, Rathbun, G, Lam, KP, Oltz, EM, Stewart, V, Mendelsohn, M *et al.* (1992). RAG-2-deficient mice lack mature lymphocytes owing to inability to initiate V(D)J rearrangement. *Cell* **68**: 855–867.
31. Cao, X, Shores, EW, Hu-Li, J, Anver, MR, Kelsall, BL, Russell, SM *et al.* (1995). Defective lymphoid development in mice lacking expression of the common cytokine receptor gamma chain. *Immunity* **2**: 223–238.
32. Armentano, D, Smith, MP, Sookdeo, CC, Zabner, J, Perricone, MA, St George, JA *et al.* (1999). E4ORF3 requirement for achieving long-term transgene expression from the cytomegalovirus promoter in adenovirus vectors. *J Virol* **73**: 7031–7034.
33. Dormond, E, Chahal, P, Bernier, A, Tran, R, Perrier, M and Kamen, A (2010). An efficient process for the purification of helper-dependent adenoviral vector and removal of helper virus by iodixanol ultracentrifugation. *J Virol Methods* **165**: 83–89.
34. Armentano, D, Zabner, J, Sacks, C, Sookdeo, CC, Smith, MP, St George, JA *et al.* (1997). Effect of the E4 region on the persistence of transgene expression from adenovirus vectors. *J Virol* **71**: 2408–2416.
35. Ylösmäki, E, Martikainen, M, Hinkkanen, A and Saksela, K (2013). Attenuation of Semliki Forest virus neurovirulence by microRNA-mediated detargeting. *J Virol* **87**: 335–344.
36. Kafri, T, Morgan, D, Krahl, T, Sarvetnick, N, Sherman, L and Verma, I (1998). Cellular immune response to adenoviral vector infected cells does not require de novo viral gene expression: implications for gene therapy. *Proc Natl Acad Sci USA* **95**: 11377–11382.
37. Roth, MD, Cheng, Q, Harui, A, Basak, SK, Mitani, K, Low, TA *et al.* (2002). Helper-dependent adenoviral vectors efficiently express transgenes in human dendritic cells but still stimulate antiviral immune responses. *J Immunol* **169**: 4651–4656.
38. Muruve, DA, Cotter, MJ, Zaiss, AK, White, LR, Liu, Q, Chan, T *et al.* (2004). Helper-dependent adenovirus vectors elicit intact innate but attenuated adaptive host immune responses in vivo. *J Virol* **78**: 5966–5972.
39. Van Linthout, S, Lusky, M, Collen, D and De Geest, B (2002). Persistent hepatic expression of human apo A-I after transfer with a helper-virus independent adenoviral vector. *Gene Ther* **9**: 1520–1528.
40. Mizuguchi, H and Kay, MA (1998). Efficient construction of a recombinant adenovirus vector by an improved *in vitro* ligation method. *Hum Gene Ther* **9**: 2577–2583.
41. Koizumi, N, Mizuguchi, H, Utoguchi, N, Watanabe, Y and Hayakawa, T (2003). Generation of fiber-modified adenovirus vectors containing heterologous peptides in both the HI loop and C terminus of the fiber knob. *J Gene Med* **5**: 267–276.
42. Mizuguchi, H and Kay, MA (1999). A simple method for constructing E1- and E1/E4-deleted recombinant adenoviral vectors. *Hum Gene Ther* **10**: 2013–2017.
43. Miao, CH, Ohashi, K, Patijn, GA, Meuse, L, Ye, X, Thompson, AR *et al.* (2000). Inclusion of the hepatic locus control region, an intron, and untranslated region increases and stabilizes hepatic factor IX gene expression *in vivo* but not *in vitro*. *Mol Ther* **1**: 522–532.
44. Maizel, JV Jr, White, DO and Scharff, MD (1968). The polypeptides of adenovirus. I. Evidence for multiple protein components in the virion and a comparison of types 2, 7A, and 12. *Virology* **36**: 115–125.
45. Suzuki, E, Murata, T, Watanabe, S, Kujime, Y, Hirose, M, Pan, J *et al.* (2004). A simple method for the simultaneous detection of E1A and E1B in adenovirus stocks. *Oncol Rep* **11**: 173–178.
46. Shimizu, K, Sakurai, F, Machitani, M, Katayama, K and Mizuguchi, H (2011). Quantitative analysis of the leaky expression of adenovirus genes in cells transduced with a replication-incompetent adenovirus vector. *Mol Pharm* **8**: 1430–1435.
47. Elmén, J, Lindow, M, Schütz, S, Lawrence, M, Petri, A, Obad, S *et al.* (2008). LNA-mediated microRNA silencing in non-human primates. *Nature* **452**: 896–899.
48. Shoji, M, Yoshizaki, S, Mizuguchi, H, Okuda, K and Shimada, M (2012). Immunogenic comparison of chimeric adenovirus 5/35 vector carrying optimized human immunodeficiency virus clade C genes and various promoters. *PLoS ONE* **7**: e30302.
49. Hutnick, NA, Carnathan, D, Demers, K, Makedonas, G, Ertl, HC and Betts, MR (2010). Adenovirus-specific human T cells are pervasive, polyfunctional, and cross-reactive. *Vaccine* **28**: 1932–1941.
50. Wang, H, Gao, X, Fukumoto, S, Tademoto, S, Sato, K and Hirai, K (1998). Post-isolation inducible nitric oxide synthase gene expression due to collagenase buffer perfusion and characterization of the gene regulation in primary cultured murine hepatocytes. *J Biochem* **124**: 892–899.
51. Kano, A, Watanabe, Y, Takeda, N, Aizawa, S and Akaike, T (1997). Analysis of IFN-gamma-induced cell cycle arrest and cell death in hepatocytes. *J Biochem* **121**: 677–683.
52. Xu, ZL, Mizuguchi, H, Ishii-Watabe, A, Uchida, E, Mayumi, T and Hayakawa, T (2001). Optimization of transcriptional regulatory elements for constructing plasmid vectors. *Gene* **272**: 149–156.

Supplementary Information accompanies this paper on the *Molecular Therapy—Methods & Clinical Development* website (http://www.nature.com/mtm)

Hindawi Publishing Corporation
BioMed Research International
Volume 2014, Article ID 158128, 6 pages
http://dx.doi.org/10.1155/2014/158128

Research Article

The Early Activation of CD8$^+$ T Cells Is Dependent on Type I IFN Signaling following Intramuscular Vaccination of Adenovirus Vector

Masahisa Hemmi,[1] Masashi Tachibana,[1] Sayaka Tsuzuki,[1] Masaki Shoji,[1] Fuminori Sakurai,[1,2] Kenji Kawabata,[3] Kouji Kobiyama,[4,5] Ken J. Ishii,[4,5] Shizuo Akira,[6,7] and Hiroyuki Mizuguchi[1,8,9,10]

[1] *Laboratory of Biochemistry and Molecular Biology, Graduate School of Pharmaceutical Sciences, Osaka University, 1-6 Yamadaoka, Suita, Osaka 565-0871, Japan*
[2] *Laboratory of Regulatory Sciences for Oligonucleotide Therapeutics, Clinical Drug Development Unit, Graduate School of Pharmaceutical Sciences, Osaka University, 1-6 Yamadaoka, Suita, Osaka 565-0871, Japan*
[3] *Laboratory of Stem Cell Regulation, National Institute of Biomedical Innovation, 7-6-8 Asagi, Saito, Ibaraki, Osaka 567-0085, Japan*
[4] *Laboratory of Adjuvant Innovation, National Institute of Biomedical Innovation, 7-6-8 Asagi, Saito, Ibaraki, Osaka 567-0085, Japan*
[5] *Laboratory of Vaccine Science, World Premier International Research Center Immunology Frontier Research Center, Osaka University, 3-1 Yamadaoka, Suita, Osaka 565-0871, Japan*
[6] *Laboratory of Host Defense, World Premier International Research Center Immunology Frontier Research Center, Osaka University, 3-1 Yamadaoka, Suita, Osaka 565-0871, Japan*
[7] *Department of Host Defense, The Research Institute for Microbial Diseases, Osaka University, 3-1 Yamadaoka, Suita, Osaka 565-0871, Japan*
[8] *iPS Cell-Based Research Project on Hepatic Toxicity and Metabolism, Graduate School of Pharmaceutical Sciences, Osaka University, 1-6 Yamadaoka, Suita, Osaka 565-0871, Japan*
[9] *Laboratory of Hepatocyte Differentiation, National Institute of Biomedical Innovation, 7-6-8 Asagi, Saito, Ibaraki, Osaka 567-0085, Japan*
[10] *The Center for Advanced Medical Engineering and Informatics, Osaka University, 2-2 Yamadaoka, Suita, Osaka 565-0871, Japan*

Correspondence should be addressed to Hiroyuki Mizuguchi; mizuguch@phs.osaka-u.ac.jp

Received 19 March 2014; Accepted 14 May 2014; Published 27 May 2014

Academic Editor: Xin Ming

Few of the vaccines in current use can induce antigen- (Ag-) specific immunity in both mucosal and systemic compartments. Hence, the development of vaccines that realize both mucosal and systemic protection against various pathogens is a high priority in global health. Recently, it has been reported that intramuscular (i.m.) vaccination of an adenovirus vector (Adv) can induce Ag-specific cytotoxic T lymphocytes (CTLs) in both systemic and gut mucosal compartments. We previously revealed that type I IFN signaling is required for the induction of gut mucosal CTLs, not systemic CTLs. However, the molecular mechanism via type I IFN signaling is largely unknown. Here, we report that type I IFN signaling following i.m. Adv vaccination is required for the expression of type I IFN in the inguinal lymph nodes (iLNs), which are the draining lymph nodes of the administration site. We also showed that the type I IFN signaling is indispensable for the early activation of CTLs in iLNs. These data suggested that type I IFN signaling has an important role in the translation of systemic innate immune response into mucosal adaptive immunity by amplifying the innate immune signaling and activating CTLs in the iLN.

1. Introduction

Mucosal membranes have enormous surface areas, through which most pathogens access the body, and therefore, they are important in vaccine development to establish protective immune responses at mucosal sites as well as systemic sites [1, 2]. Hence, the development of vaccines that realize both

mucosal and systemic protection against various pathogens is a high priority in global health. However, few of the vaccines in current use can induce antigen- (Ag-) specific immunity in both mucosal and systemic compartments [3]. In general, the induction of mucosal immunity by systemic administration of vaccine has proven to be difficult due to the unique immunological features of the mucosal immune system [3].

The replication incompetent recombinant adenovirus vector (Adv) has several advantages as a gene therapy vector: it provides the highest gene transduction efficiency among the currently available vectors, it has low genotoxicity because it is not integrated into the chromosomal DNA, and it can be easily prepared in high titers. Moreover, it has been revealed that Adv can be applied to gene therapy-based vaccines, and several Adv and vaccine protocols have been used in preclinical studies [4]. Recently, it has been reported that intramuscular (i.m.) immunization with an Adv vaccine-expressing simian immunodeficiency virus (SIV) gag can induce functional and sustainable SIV gag-specific cytotoxic T lymphocytes (CTLs) in the gut mucosal compartments as well as the systemic compartments in mice and rhesus macaques [5–7]. Adv is expected to become a next generation mucosal vaccine that combats severe intracellular pathogens [8].

Innate immune responses have been clearly shown to be critical for the optimal induction of adaptive immune responses [9–11]. Moreover, there is accumulating evidence that the adjuvants which activate innate immunity are effective for the induction of vaccine effects [12]. Several studies have revealed that Adv-derived nucleic acids, adenoviral genomic DNA, and adenoviral noncoding RNA (virus-associated RNA (VA-RNA)) activate innate immunity and produce innate immune cytokines. The adenoviral genomic DNA triggers innate immune responses through several pattern recognition receptors and adaptor molecules, such as Toll-like receptor 9 (TLR9)/myeloid differentiation primary-response protein 88 (MyD88) [13–15], and cGAMP synthase (cGAS)/stimulator of interferon genes (STING) [16], and induces the production of type I IFNs and proinflammatory cytokines. VA-RNA also induces the production of type I IFN through IFN-β promoter stimulator-1 (IPS-1) [17]. Type I IFN induced by Adv immunization has been shown to have an important role in the subsequent systemic adaptive immunity. It is indicated that not only dendritic cells (DCs), but also other types of cells, such as stromal cells, produce IFN-β *in vivo* and are involved in the induction of adaptive immunity [17–19]. Thus, determining the role of IFN-β *in vivo* is important for vaccine development. Moreover, the magnitudes of type I IFN correlate with the titers of Ad-specific neutralizing antibodies, suggesting that type I IFN signaling controls the efficacy of Adv vaccine [20]. We previously reported that type I IFN signaling following i.m. Adv vaccination is required for the induction of Ag-specific CTLs not in the systemic compartment but in the gut mucosal compartment [8]. Thus, type I IFN is important for the positive regulation of the Ag-specific gut mucosal cellular immune response. However, it is unclear how the Adv-induced type I IFN signaling translates innate immune response into gut mucosal adaptive immunity.

In this study, we report that type I IFN signaling is indispensable for the expression of IFN-α, IFN-β, cGAS, and TLR9in the draining lymph nodes (DLNs) in the early stage following i.m. Adv vaccination. Moreover, we found that type I IFN signaling is essential for the early activation of $CD8^+$ T cells in the DLNs. These data suggested that type I IFN signaling has an important role in the translation of systemic innate immunity into mucosal adaptive immunity. Our findings should lead to the development of safer and more efficient mucosal Adv vaccines.

2. Materials and Methods

2.1. Mice. C57BL/6J (wild-type, WT) mice were purchased from Japan SLC (Hamamatsu, Japan) and $IFNAR2^{-/-}$mice (C57BL/6J background) were established as described previously [21]. All mice were housed in an animal facility under specific pathogen-free conditions and used at 7-8 weeks of age. All animal experimental procedures used in this study were performed in accordance with the institutional guidelines for animal experiments at Osaka University and the National Institute of Biomedical Innovation.

2.2. Adv Production and Immunization. The adenovirus type 5 vector-expressing LacZ (Ad-LacZ) was constructed as described previously [22]. Briefly, the expression cassette containing the chicken β-actin promoter with the cytomegalovirus enhancer (CA) driven [23] LacZ gene was inserted into the E1/E3-deleted adenovirus type 5 genome. This virus was grown in 293 cells using standard techniques. Ad-LacZ was purified with $CsCl_2$ step gradient ultracentrifugation, dialyzed with a solution containing 10 mM Tris (pH 7.5), 1 mM $MgCl_2$, and 10% glycerol, and stored in aliquots at −80°C. Determination of the virus particle (vp) titers was accomplished spectrophotometrically according to the methods of Maizel et al. [24]. All mice were injected under anesthesia in the right and left quadriceps muscles with Ad-LacZ (5×10^9 vp per muscle; total 10^{10} vp per mouse).

2.3. Isolation of Mononuclear Cells. The inguinal lymph nodes and mesenteric lymph nodes were dissected and pressed through a 70 μm cell strainer. The cells were washed with FACS buffer (2% FCS, 0.02% sodium azide in PBS).

2.4. DNA Isolation and qPCR. Total DNA was isolated from whole tissues using a DNeasy Blood & Tissue Kit (QIAGEN). Quantitative PCR was performed with Taqman Fast Universal PCR Master Mix (Applied Biosystems) using an Applied Biosystem StepOnePlus Real-Time PCR System. Absolute quantities were calculated using standard curves. The copy numbers of each gene were normalized with those of GAPDH. The primer sequences in this study are Gapdh forward, 5′-CAATGTGTCCGTCGTGGATCT-3′; Gapdh reverse, 5′-GTCCTCAGTGTAGCCCAAGATG-3′; Ad E4 forward, 5′-GGGATCGTCTACCTCCTTTTGA-3′; Ad E4 reverse, 5′-GGGCAGCAGCGGATGAT-3′.

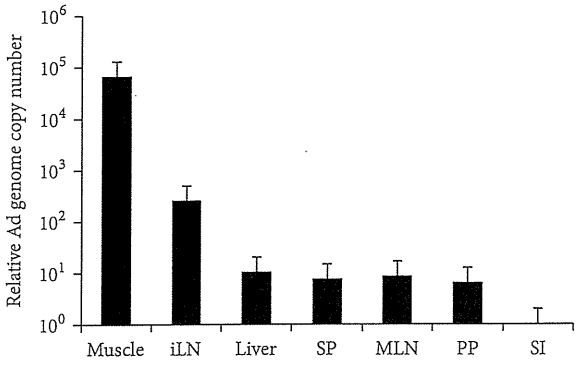

FIGURE 1: The tissue distribution of Adv following i.m. Adv vaccination. At 8 hours after the i.m. vaccination of 10^{10} vp of Ad-LacZ, the tissue distribution of Adv was determined by the absolute quantity of Ad E4 gene in each tissue, normalized by the copy number of GAPDH. The graphs represent the relative Ad genome copy number in each tissue normalized by that of the small intestine. Data are shown as the means ± S.E.M. (n = 3). iLN, inguinal lymph node; SP, spleen; MLN, mesenteric lymph node; PP, Peyer's patch; SI, small intestine.

2.5. RNA Isolation and RT-PCR. Total RNA was isolated from mononuclear cells using ISOGEN (Nippon Gene). cDNA was synthesized using 400 ng of total RNA with a Superscript VILO cDNA Synthesis Kit (Invitrogen) according to the manufacturer's instructions. Quantitative RT-PCR was performed with THUNDERBIRD qPCR Mix (TOYOBO) using an Applied Biosystem StepOnePlus Real-Time PCR System. Relative expression was calculated using the $\Delta\Delta C_T$ method. The mRNA level of each gene was normalized with that of β-actin. The primer sequences used in this study are *Actb* forward, 5′-GGCTGTATTCCCCTCCATCG-3′; *Actb* reverse, 5′-CCAGTTGGTAACAATGCCATGT-3′; *Ifna* forward, 5′-CTTCCACAGGATCACTGTGTACCT-3′; *Ifna* reverse, 5′-TTCTGCTCTGACCACCTCCC-3′; *Ifnb* forward, 5′-CTGGAGCAGCTGAATGGAAAG-3′; *Ifnb* reverse, 5′-CTTCTCCGTCATCTCCATAGGG-3′; *Mb21d1* forward, 5′-AGGAAGCCCTGCTGTAACACTTCT-3′; *Mb21d1* reverse, 5′-AGCCAGCCTTGAATAGGTAGTCCT-3′; *Tlr9* forward, 5′-ATGGTTCTCCGTCGAAGGACT-3′; *Tlr9* reverse, 5′-GAGGCTTCAGCTCACAGGG-3′; *Ddx41* forward, 5′-AGTCCGCCAAGGAAAAGCAA-3′; *Ddx41* reverse, 5′-CTCAGACATGCTCAGGACATAAC-3′; *Il1b* forward, 5′-GCAGCAGCACATCAACAAG-3′; *Il1b* reverse, 5′-CGGGAAAGACACAGGTAGC-3′; *Tnfa* forward, 5′-CCCTCACACTCAGATCATCTTCT-3′; *Tnfa* reverse, 5′-GCTACGACGTGGGCTACAG-3′.

2.6. Flow Cytometry. The antimouse antibodies used in this study were purchased from eBioscience (PE-Cy7-CD3ε (145-2C11)) and BioLegend (FITC-CD4 (GK1.5), APC-Cy7-CD8α (53-6.7), Pacific Blue-CD69 (H1.2F3)). Flow cytometry analysis was performed using a fluorescence-activated cell sorting (FACS) LSR Fortessa flow cytometer and BD FACSDiva software (BD Bioscience). Dead cells were excluded by 7-amino-actinomycin D staining (eBioscience).

2.7. Statistics. All results are shown as the mean ± standard error of the mean. Statistical significance was analyzed by the One-way ANOVA among groups.

3. Results

3.1. Adv Was Mainly Distributed to the Inguinal Lymph Nodes following i.m. Adv Vaccination. Innate immune responses are elicited within several hours after i.m. Adv vaccination. To reveal the sites where Adv induces the responses, we first examined Ad genome copy numbers in each tissue at 8 hours after i.m. Adv vaccination. Adv was mainly distributed to the muscles and inguinal lymph nodes (iLNs), the DLNs of the vaccination site (Figure 1). On the other hand, Adv was barely distributed to mesenteric lymph node (MLN), which is important for gut mucosal immunity. The distributions of Adv in the liver, spleen (SP), Peyer's patches (PP), and small intestine (SI) were similar to those in the MLN. These results suggested that Adv should induce innate immune responses in the iLNs.

3.2. Type I IFN Signaling Enhances the Expression of Innate Immune Cytokines and DNA Sensors in the Draining Lymph Nodes. Next, to reveal the roles of type I IFN signaling in the induction of gut mucosal CTLs, we examined the expression of innate immune cytokines and interferon-stimulated genes (ISGs) in iLNs and MLN by using type I IFN receptor knockout (IFNAR2 KO) mice, which have defects in immune responses to viruses and double-stranded DNA. In Adv-administrated WT mice, the expression of IFN-α and IFN-β was upregulated in the iLNs, where Adv was mainly distributed at this time point (Figure 2(a)). Moreover, in Adv-administrated WT mice, the expression of IL-1β and TNF-α tended to be upregulated in the iLNs (Figure 2(a)). On the other hand, the expression of these cytokines was not upregulated in the MLN, where Adv was barely distributed. Similarly, the expression of cGAS, a representative ISG, that is, encoded by *Mb21d1* [25], was upregulated in the iLNs (Figure 2(b)). However, in Adv-administrated IFNAR2 KO mice, the expression of IFN-α, IFN-β, and cGAS in the iLNs was not upregulated following i.m. Adv vaccination. In addition, in Adv-administrated IFNAR2 KO mice, the expression of IL-1β and TNF-α in the iLNs was lower than that in the iLNs of Adv-administrated WT mice.

Since cGAS is one of the DNA sensors detecting Ad genome [16], we next examined the expression of other DNA sensors, TLR9 and DDX41, which are widely known for sensing Ad genome [15, 26]. In Adv-administrated WT mice, only the expression of TLR9 was upregulated in the iLNs (Figure 2(c)). However, it was not upregulated in the iLNs of Adv-administrated IFNAR2 KO mice. These data suggested that type I IFN signaling enhances the expression of IFN-α, IFN-β, cGAS, and TLR9 in the iLNs, where much Adv is distributed from the muscles. It is speculated that the lack of type I IFN signaling in the innate immune responses at the iLNs leads to the significant reduction of antigen-specific CTLs in the gut mucosal compartment.

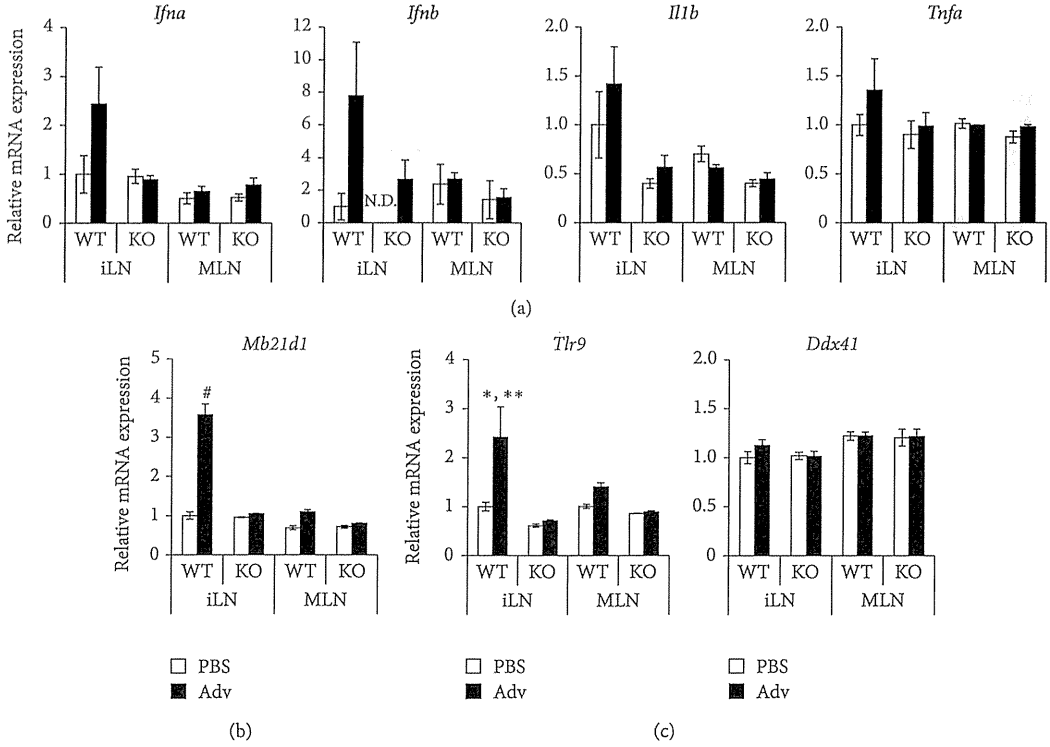

FIGURE 2: Relative mRNA expressions in the iLNs and MLN of WT and IFNAR2 KO mice following i.m. Adv vaccination. At 8 hours after the i.m. vaccination of 10^{10} vp of Ad-LacZ, total RNA was extracted from mononuclear cells in the LNs of each mouse. The mRNA expressions of *Ifna*, *Ifnb*, *Il1b*, *Tnfa* (a), *Mb21d1* (b), *Tlr9*, and *Ddx41* (c) in the LNs were measured by qRT-PCR, normalized by *Actb*. The graphs represent the relative mRNA expression of each gene normalized by that of PBS-administrated WT mice. Data are shown as the means ± S.E.M. ($n = 3$) and are representative of two independent experiments. $^{*}P < 0.05$ compared with other groups except for the MLN of Adv-administrated WT mice. $^{**}P < 0.01$ compared with the iLNs of IFNAR2 KO mice. $^{\#}P < 0.0001$ compared with other groups.

3.3. Type I IFN Signaling Is Required for the Early Activation of CTLs in iLNs. Since type I IFN signaling was not induced in IFNAR2 KO mice following i.m. Adv vaccination, we hypothesized that the early activation of T cells is not elicited sufficiently in IFNAR2 KO mice. After antigenic stimulation, T cells express a series of several activation markers, including CD69, CD44, and CD25, dependent on the developmental stages from naïve to effector. To examine whether the type I IFN signaling following i.m. Adv vaccination has an effect on an early activation marker, CD69 [27, 28], on $CD8^+$ T cells, we estimated the frequencies of $CD69^+$ cells in $CD8^+$ T cells residing in the DLNs. In Adv-administrated WT mice, the frequencies of $CD69^+$ cells in $CD8^+$ T cells in the iLNs were increased, while those in the MLN were not. However, in the case of Adv-administrated IFNAR2 KO mice, the frequencies of $CD69^+$ cells in $CD8^+$ T cells in the iLNs were significantly reduced compared with those of Adv-administrated WT mice (Figure 3). Thus, these data correlate with the results shown in Figure 2, in which the type I IFN response was elicited at the iLNs and diminished in IFNAR2 KO mice. These results indicated that type I IFN signaling induces the expression of CD69 on $CD8^+$ T cells in Adv-administrated mice. Collectively, these data suggest that the early activation of $CD8^+$ T cells via type I IFN signaling promotes the induction and/or migration of gut mucosal Ag-specific CTLs.

4. Discussion

In this study, we demonstrated that type I IFN signaling following i.m. Adv vaccination promotes the expression of IFN-α, IFN-β, and cGAS in the iLNs where Adv is mainly distributed at this time point and strongly induces the expression of CD69 on $CD8^+$ T cells in the iLNs. The expression of type I IFN is amplified through IFNAR [29, 30]. Therefore, it is reasonable that the expression of type I IFN is decreased in IFNAR2 KO mice. We observed that IFN-β expression was more strongly induced by type I IFN signaling than IFN-α expression. It has been reported that IFN-α is mainly produced by plasmacytoid dendritic cells (pDCs), while IFN-β is mainly produced by myeloid DCs (mDCs) and mouse embryonic fibroblasts (MEFs) [17, 31, 32]. Hence, it is speculated that type I IFN signaling contributes to IFN-β production from DCs and fibroblasts in the iLNs, such as stromal cells, following i.m. Adv vaccination. In addition, we observed a significant reduction in TLR9 expression as well as cGAS expression in IFNAR2 KO mice. cGAS and TLR9 have been reported to be the DNA sensors responsible for the

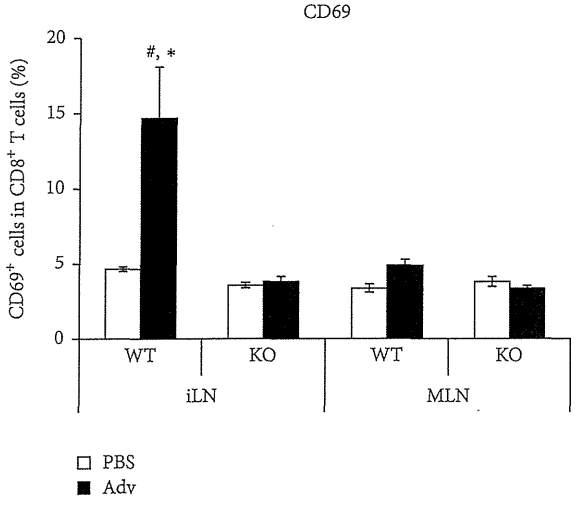

FIGURE 3: The frequencies of early activated $CD8^+$ T cells in the iLNs and MLN of WT and IFNAR2 KO mice following i.m. Adv vaccination. At 24 hours after the i.m. vaccination of 10^{10} vp of Ad-LacZ, the frequencies of $CD69^+$ T cells in $CD8^+$ T cells in the LNs of each mouse were measured by flow cytometry. Data are the pools of three independent experiments and are shown as the means ± S.E.M. ($n = 6$). $^*P < 0.001$ compared with the iLNs of PBS-administrated WT mice and MLN of Adv-administrated WT mice. $^\#P < 0.0001$ compared with other groups.

recognition of adenoviral DNA leading to the induction of type I IFN production [15, 16]. It is speculated that type I IFN signaling promotes the detection of Adv by cGAS and TLR9 and amplifies their signaling *in vivo*.

Recently, Weerd et al. revealed that IFN-β binds to the low-affinity component of IFNAR, IFNAR1, in the absence of IFNAR2 [33]. Moreover, IFNAR1-IFN-β complex activates unique intracellular signaling. However, in our study, we did not observe such phenomenon in IFNAR2 KO mice. For example, Weerd et al. showed that in IFNAR2 KO peritoneal exudate cells (PECs), IL-1β expression was upregulated 13.5-fold by IFN-β compared to nontreated IFNAR2 KO PECs. On the other hand, in our study, IL-1β expression in the iLNs of Adv-administrated IFNAR2 KO mice was upregulated just only 1.42-fold as much as that of PBS-administrated IFNAR2 KO mice (Figure 2(a)). Thus, it is speculated that the level of IFN-β in our study would be much lower than that in their study and the IFN-β signaling in our study would be transmitted via IFNAR2, which is the high-affinity component of IFNAR.

We observed a significant reduction of CD69 expression on $CD8^+$ T cells in the iLNs of IFNAR2 KO mice following i.m. Adv vaccination. Our results are consistent with a previous report that the expression of CD69 is strongly induced by type I IFN [34, 35]. CD69 inhibits egress of T cells from the spleen and secondary lymphoid tissues during T cell maturation [35]. It is speculated that the reduction of CD69 expression in IFNAR2 KO mice induces egress of $CD8^+$ T cells from the iLNs in the early stage of T cell maturation. In consequence, activated $CD8^+$ T cells in the iLNs fail to mature sufficiently, and thus, these cells do not acquire a gut-homing capacity. Moreover, Alari-Pahissa et al. recently reported that CD69 does not affect $CD8^+$ T cell priming following Ag-expressing vaccinia virus vector immunization [36]. Considering our previous finding that systemic Ag-specific CTLs are induced in IFNAR2 KO mice following i.m. Adv vaccination as similar as WT mice [8], it is likely that the reduction of CD69 expression on $CD8^+$ T cells does not alter $CD8^+$ T cell priming. For these reasons, it is suggested that type I IFN signaling-induced CD69 expression on $CD8^+$ T cells might regulate Ag-specific CTLs in the gut mucosal compartment.

In summary, we have shown the molecular mechanism of the induction of gut mucosal CTLs following i.m. Adv vaccination. We found that type I IFN signaling is required for the production of large amounts of type I IFN and the upregulation of CD69 on $CD8^+$ T cells in the iLNs. Our findings should contribute to the development of more efficient and safer mucosal vaccines and adjuvants.

Conflict of Interests

The authors declare that there is no conflict of interests regarding the publication of this paper.

Authors' Contribution

Masahisa Hemmi and Masashi Tachibana contributed equally to this paper.

Acknowledgment

This work was supported by grants from the Ministry of Health, Labour, and Welfare of Japan.

References

[1] J. Holmgren and C. Czerkinsky, "Mucosal immunity and vaccines," *Nature Medicine*, vol. 11, no. 4, pp. S45–S53, 2005.

[2] I. M. Belyakov and J. D. Ahlers, "Functional $CD8^+$ CTLs in mucosal sites and HIV infection: moving forward toward a mucosal AIDS vaccine," *Trends in Immunology*, vol. 29, no. 11, pp. 574–585, 2008.

[3] M. R. Neutra and P. A. Kozlowski, "Mucosal vaccines: the promise and the challenge," *Nature Reviews Immunology*, vol. 6, no. 2, pp. 148–158, 2006.

[4] N. Tatsis and H. C. J. Ertl, "Adenoviruses as vaccine vectors," *Molecular Therapy*, vol. 10, no. 4, pp. 616–629, 2004.

[5] D. R. Kaufman, J. Liu, A. Carville et al., "Trafficking of antigen-specific $CD8^+$ T lymphocytes to mucosal surfaces following intramuscular vaccination," *The Journal of Immunology*, vol. 181, no. 6, pp. 4188–4198, 2008.

[6] D. R. Kaufman, M. Bivas-Benita, N. L. Simmons, D. Miller, and D. H. Barouch, "Route of adenovirus-based HIV-1 vaccine delivery impacts the phenotype and trafficking of vaccine-elicited $CD8^+$ T lymphocytes," *Journal of Virology*, vol. 84, no. 12, pp. 5986–5996, 2010.

[7] S. Ganguly, S. Manicassamy, J. Blackwell, B. Pulendran, and R. R. Amara, "Adenovirus type 5 induces vitamin A-metabolizing

enzymes in dendritic cells and enhances priming of gut-homing CD8 T cells," *Mucosal Immunology*, vol. 4, no. 5, pp. 528–538, 2011.

[8] M. Shoji, M. Tachibana, K. Katayama et al., "Type-I IFN signaling is required for the induction of antigen-specific $CD8^+$ T cell responses by adenovirus vector vaccine in the gut-mucosa," *Biochemical and Biophysical Research Communications*, vol. 425, no. 1, pp. 89–93, 2012.

[9] T. Kawai and S. Akira, "Toll-like receptors and their crosstalk with other innate receptors in infection and immunity," *Immunity*, vol. 34, no. 5, pp. 637–650, 2011.

[10] O. Takeuchi and S. Akira, "Pattern recognition receptors and inflammation," *Cell*, vol. 140, no. 6, pp. 805–820, 2010.

[11] T. Kawai and S. Akira, "Innate immune recognition of viral infection," *Nature Immunology*, vol. 7, no. 2, pp. 131–137, 2006.

[12] B. Pulendran and R. Ahmed, "Translating innate immunity into immunological memory: implications for vaccine development," *Cell*, vol. 124, no. 4, pp. 849–863, 2006.

[13] Z. C. Hartman, A. Kiang, R. S. Everett et al., "Adenovirus infection triggers a rapid, MyD88-regulated transcriptome response critical to acute-phase and adaptive immune responses in vivo," *Journal of Virology*, vol. 81, no. 4, pp. 1796–1812, 2007.

[14] J. Zhu, X. Huang, and Y. Yang, "Innate immune response to adenoviral vectors is mediated by both Toll-like receptor-dependent and -independent pathways," *Journal of Virology*, vol. 81, no. 7, pp. 3170–3180, 2007.

[15] T. Yamaguchi, K. Kawabata, N. Koizumi et al., "Role of MyD88 and TLR9 in the innate immune response elicited by serotype 5 adenoviral vectors," *Human Gene Therapy*, vol. 18, no. 8, pp. 753–762, 2007.

[16] E. Lam, S. Stein, and E. Falck-Pedersen, "Adenovirus detection by the cGAS/STING/TBK1 DNA sensing cascade," *Journal of Virology*, vol. 88, no. 2, pp. 974–981, 2014.

[17] T. Yamaguchi, K. Kawabata, E. Kouyama et al., "Induction of type I interferon by adenovirus-encoded small RNAs," *Proceedings of the National Academy of Sciences of the United States of America*, vol. 107, no. 40, pp. 17286–17291, 2010.

[18] S. E. Hensley, W. Giles-Davis, K. C. McCoy, W. Weninger, and H. C. J. Ertl, "Dendritic cell maturation, but not $CD8^+$ T cell induction, is dependent on type I IFN signaling during vaccination with adenovirus vectors," *The Journal of Immunology*, vol. 175, no. 9, pp. 6032–6041, 2005.

[19] S. N. Mueller and R. N. Germain, "Stromal cell contributions to the homeostasis and functionality of the immune system," *Nature Reviews Immunology*, vol. 9, no. 9, pp. 618–629, 2009.

[20] M. Perreau, H. C. Welles, C. Pellaton et al., "The number of toll-like receptor 9-agonist motifs in the adenovirus genome correlates with induction of dendritic cell maturation by adenovirus immune complexes," *Journal of Virology*, vol. 86, no. 11, pp. 6279–6285, 2012.

[21] K. J. Ishii, T. Kawagoe, S. Koyama et al., "TANK-binding kinase-1 delineates innate and adaptive immune responses to DNA vaccines," *Nature*, vol. 451, no. 7179, pp. 725–729, 2008.

[22] K. Kawabata, F. Sakurai, T. Yamaguchi, T. Hayakawa, and H. Mizuguchi, "Efficient gene transfer into mouse embryonic stem cells with adenovirus vectors," *Molecular Therapy*, vol. 12, no. 3, pp. 547–554, 2005.

[23] N. Hitoshi, Y. Ken-ichi, and M. Jun-ichi, "Efficient selection for high-expression transfectants with a novel eukaryotic vector," *Gene*, vol. 108, no. 2, pp. 193–199, 1991.

[24] J. V. Maizel Jr., D. O. White, and M. D. Scharff, "The polypeptides of adenovirus. I. Evidence for multiple protein components in the virion and a comparison of types 2, 7A, and 12," *Virology*, vol. 36, no. 1, pp. 115–125, 1968.

[25] J. W. Schoggins, S. J. Wilson, M. Panis et al., "A diverse range of gene products are effectors of the type I interferon antiviral response," *Nature*, vol. 472, no. 7344, pp. 481–485, 2011.

[26] Z. Zhang, B. Yuan, M. Bao, N. Lu, T. Kim, and Y.-J. Liu, "The helicase DDX41 senses intracellular DNA mediated by the adaptor STING in dendritic cells," *Nature Immunology*, vol. 12, no. 10, pp. 959–965, 2011.

[27] J. F. Krowka, B. Cuevas, D. C. Maron, K. S. Steimer, M. S. Ascher, and H. W. Sheppard, "Expression of CD69 after in vitro stimulation: a rapid method for quantitating impaired lymphocyte responses in HIV-infected individuals," *Journal of Acquired Immune Deficiency Syndromes and Human Retrovirology*, vol. 11, no. 1, pp. 95–104, 1996.

[28] P. E. Simms and T. M. Ellis, "Utility of flow cytometric detection of CD69 expression as a rapid method for determining poly- and oligoclonal lymphocyte activation," *Clinical and Diagnostic Laboratory Immunology*, vol. 3, no. 3, pp. 301–304, 1996.

[29] I. Marié, J. E. Durbin, and D. E. Levy, "Differential viral induction of distinct interferon-α genes by positive feedback through interferon regulatory factor-7," *The EMBO Journal*, vol. 17, no. 22, pp. 6660–6669, 1998.

[30] M. Dalod, T. Hamilton, R. Salomon et al., "Dendritic cell responses to early murine cytomegalovirus infection: subset functional specialization and differential regulation by interferon α/β," *The Journal of Experimental Medicine*, vol. 197, no. 7, pp. 885–898, 2003.

[31] E. Basner-Tschakarjan, E. Gaffal, M. O'Keeffe et al., "Adenovirus efficiently transduces plasmacytoid dendritic cells resulting in TLR9-dependent maturation and IFN-α production," *Journal of Gene Medicine*, vol. 8, no. 11, pp. 1300–1306, 2006.

[32] G. Fejer, L. Drechsel, J. Liese et al., "Key role of splenic myeloid DCs in the IFN-$\alpha\beta$ response to adenoviruses in Vivo," *PLoS Pathogens*, vol. 4, no. 11, Article ID e1000208, 2008.

[33] N. A. de Weerd, J. P. Vivian, T. K. Nguyen et al., "Structural basis of a unique interferon-β signaling axis mediated via the receptor IFNAR1," *Nature Immunology*, vol. 14, no. 9, pp. 901–907, 2013.

[34] K. Radulovic, C. Manta, V. Rossini et al., "CD69 regulates type I IFN-induced tolerogenic signals to mucosal CD4 T cells that attenuate their colitogenic potential," *The Journal of Immunology*, vol. 188, no. 4, pp. 2001–2013, 2012.

[35] L. R. Shiow, D. B. Rosen, N. Brdičková et al., "CD69 acts downstream of interferon-α/β to inhibit S1P 1 and lymphocyte egress from lymphoid organs," *Nature*, vol. 440, no. 7083, pp. 540–544, 2006.

[36] E. Alari-Pahissa, L. Notario, E. Lorente et al., "CD69 does not affect the extent of T cell priming," *PLoS ONE*, vol. 7, no. 10, Article ID e48593, 2012.

Herpes simplex viral-vector design for efficient transduction of nonneuronal cells without cytotoxicity

Yoshitaka Miyagawa[a], Pietro Marino[a,b], Gianluca Verlengia[a,b], Hiroaki Uchida[a,1], William F. Goins[a], Shinichiro Yokota[c], David A. Geller[c,d], Osamu Yoshida[c], Joseph Mester[e], Justus B. Cohen[a], and Joseph C. Glorioso[a,2]

[a]Department of Microbiology and Molecular Genetics, University of Pittsburgh School of Medicine, Pittsburgh, PA 15219; [b]Section of Pharmacology, Department of Medical Sciences, University of Ferrara, 44121 Ferrara, Italy; [c]Thomas E. Starzl Transplantation Institute, Department of Surgery, University of Pittsburgh School of Medicine, Pittsburgh, PA 15261; [d]Liver Cancer Center, University of Pittsburgh School of Medicine, Pittsburgh, PA 15213; and [e]Department of Biological Sciences, Northern Kentucky University, Highland Heights, KY 41099

Edited by Kenneth I. Berns, University of Florida College of Medicine, Gainesville, FL, and approved February 24, 2015 (received for review December 10, 2014)

The design of highly defective herpes simplex virus (HSV) vectors for transgene expression in nonneuronal cells in the absence of toxic viral-gene activity has been elusive. Here, we report that elements of the latency locus protect a nonviral promoter against silencing in primary human cells in the absence of any viral-gene expression. We identified a CTCF motif cluster 5′ to the latency promoter and a known long-term regulatory region as important elements for vigorous transgene expression from a vector that is functionally deleted for all five immediate-early genes and the 15-kb internal repeat region. We inserted a 16.5-kb expression cassette for full-length mouse dystrophin and report robust and durable expression in dystrophin-deficient muscle cells in vitro. Given the broad cell tropism of HSV, our design provides a nontoxic vector that can accommodate large transgene constructs for transduction of a wide variety of cells without vector integration, thereby filling an important void in the current arsenal of gene-therapy vectors.

HSV vector | gene therapy | ICP0 | insulator | dystrophin

One of the limitations of promising viral-gene transfer vectors, including lentivirus, adeno-associated virus (AAV), and adenovirus vectors, is their small genome-packaging capacity (≤8 kb) (1), which precludes the incorporation of large or multiple therapeutic transgene cassettes (2–4). The large, double-stranded DNA genome of herpes simplex virus (HSV; ~152 kb) contains a substantial number of genes that are not required for infection, and redundant genes located in the repeats flanking the unique long (U_L) and short (U_S) segments of the viral genome represent additional regions that can be deleted without significant loss of infectivity. Although HSV is a neurotropic virus, inasmuch as it establishes natural latency in neurons, it is capable of infecting a wide range of cells with high efficiency, suggesting its potential for broad use as a gene-therapy vector. The goal of this research was to create a vector capable of long-term persistence and extended transgene expression in nondividing, nonneuronal cells without toxicity for the transduced cell or potential rescue of replicating virus.

HSV-1 initiates a cascade of viral-gene expression that begins with the expression of five immediate early (IE or α) genes. Two of these genes, infected cell polypeptide (ICP) 4 and ICP27, are essential for entry into the lytic-virus replication cycle, and HSV gene-delivery vectors are therefore typically deleted for one or both of these genes to mimic the latent state in sensory neurons without the possibility of reactivation. In addition, the expression of toxic nonessential IE genes, ICP0 and ICP22, has been down-regulated by promoter manipulation or blocked by deletion (5–11). The complete elimination of vector toxicity for nonneuronal cells achieved by silencing all four of these IE genes results in quiescent intranuclear episomal genomes that are diluted over time in dividing cells but persist in nondividing cells (12–14). However, transgene expression is also rapidly extinguished. Quiescence is due to global epigenetic silencing of the viral genome and can be reversed by ectopic expression of ICP0 (15, 16). To allow foreign gene expression without restoring ICP0, the transgene must be selectively protected against epigenetic silencing.

Viruses that are deleted for the ICP4 and ICP27 genes can be grown on complementing cells engineered to produce the cognate essential gene products upon virus infection (7). However, robust amplification of viruses that are in addition deleted for the ICP0 gene requires further complementation. Stable maintenance of cell lines that inducibly express all three IE genes has been a challenge due to leaky expression of the highly toxic ICP0 protein (10).

In the present study, we used HSV–bacterial artificial chromosome (BAC) recombineering to reconstruct a previous replication-defective vector that expressed a low level of ICP0, was capable of robust transient transgene expression, and displayed minimal disturbance of mouse embryonic stem cell developmental gene expression (17). In agreement with studies by others (10, 13, 18), we found that complete elimination of ICP0 expression was required to limit vector toxicity for human fibroblasts and that both viral-gene expression and transgene expression were essentially abolished in this situation. To facilitate consistent vector growth, we constructed a cell line that stably and efficiently complements the multiple IE gene defects in this type of vector. We show that a heterologous promoter–reporter gene expression cassette remains transcriptionally active in human dermal fibroblasts (HDFs) when located in the latency-associated transcript (LAT) locus but is silenced on deletion of a neighboring element

Significance

Gene therapy has made significant strides in the treatment and even cure of single-gene defects. However, the maturation of this field will require more sophisticated vehicles capable of cell-selective delivery of large genetic payloads whose regulated expression will restore or enhance cellular functionality. High-capacity herpes simplex virus vectors have the potential to meet these challenges but have been limited by the need to preserve one particularly cytotoxic viral product, infected cell polypeptide 0, to maintain transgene transcriptional activity. Our study describes a vector design that solves this conundrum, thereby promising the near-term availability of viral vectors that can efficiently deliver large or multiple regulated transgenes to a diversity of cells without attendant cytotoxicity.

Author contributions: Y.M., J.B.C., and J.C.G. designed research; Y.M., P.M., G.V., H.U., W.F.G., S.Y., O.Y., and J.M. performed research; D.A.G. contributed new reagents/analytic tools; Y.M., J.B.C., and J.C.G. analyzed data; and Y.M., J.B.C., and J.C.G. wrote the paper.

The authors declare no conflict of interest.

This article is a PNAS Direct Submission.

[1]Present address: Division of Bioengineering, Advanced Clinical Research Center, Institute of Medical Science, University of Tokyo, Tokyo 108-8639, Japan.

[2]To whom correspondence should be addressed. Email: glorioso@pitt.edu.

This article contains supporting information online at www.pnas.org/lookup/suppl/doi:10.1073/pnas.1423556112/-/DCSupplemental.

rich in CTCF-binding motifs, designated CTRL [CCCTC binding protein (CTCF) repeat long (CTRL)] (19), and the enhancer-like latency active promoter 2 (LAP2 or LATP2) region. Reporter-gene expression was also observed when the transgene cassette with LAT elements was moved to other positions in a silent-vector genome, but omission of the LAT elements abolished expression. We present evidence that these results are not unique to HDFs but also apply to other nonneuronal primary human cells. Lastly, we show that residual cytotoxicity observed with these vectors is eliminated by deletion of the BAC region, and we illustrate the potential of our findings by documenting vector-mediated expression of full-length dystrophin through at least 7 d. Together, these results hold the promise of significantly expanding the utility of HSV gene-transfer vectors to include a wide range of nonneuronal cells.

Results

Vector Engineering and Virus Growth. We used Red-mediated recombineering in bacteria (20) to generate an HSV–BAC construct, JΔNI5, that was deleted for the ICP0, ICP4, and ICP27 IE genes, the promoter and translation initiation codon of the ICP47 IE gene as part of a deletion that included the entire internal repeat (joint) region between the two unique segments (U_L, U_S) of the viral genome, and the consensus VP16-binding (TAATGARAT) motifs in the ICP22 IE gene regulatory region to change the expression kinetics of this gene to that of an early (E or β) gene (Fig. 1*A*). To convert this BAC construct to infectious virus, we created a novel U2OS-based cell line, U2OS-ICP4/27, that permanently expresses ICP4 and produces ICP27 in response to infection with an ICP4/ICP27-deleted virus (Fig. 1*B*); U2OS cells naturally complement ICP0 (21), eliminating the need to express this toxic protein. We performed a series of experiments to confirm the anticipated characteristics of JΔNI5 in comparison with two control viruses, JΔNI2 and JΔNI3, that had been produced as less debilitated predecessors of JΔNI5. JΔNI2 contained the intact coding regions of ICP0 and ICP27 under the control of copies of the early HSV thymidine kinase (TK) promoter (β0/β27) whereas, in JΔNI3, the ICP0 gene was deleted (Fig. 1*A*). In all three JΔNI viruses, an mCherry reporter-gene expression cassette was present at the position of the deleted ICP4 locus in the U_S terminal repeat, and the glycoprotein B gene was replaced with a hyperactive allele, gB:N/T (22), to enhance virus entry into cells. The genotypes of these virus constructs and all other HSV vectors generated in this study are summarized in Table 1. The biological titers in plaque-forming units (pfu) per milliliter and physical titers in viral genome copies (gc)/mL of the virus stocks used in this work are listed in Table 2.

BAC transfection and virus-growth curves confirmed the distinct complementation requirements of the three viruses (Fig. S1). Also consistent with the genetic differences between these three viruses, immunoblotting for IE gene products after infection of noncomplementing HDFs detected ICP27 in both JΔNI2- and JΔNI3-infected cells, a low level of ICP0 only in JΔNI2-infected cells, and no products in JΔNI5-infected cells (Fig. 1*C*). At 2 h postinfection (hpi), viral DNA levels in the nuclei of HDFs infected with equal gc of the 3 JΔNI viruses were similar while infections with equal pfu resulted in dissimilar nuclear gc levels (Fig. 1*D*), validating the use of gc titers to standardize virus input for comparisons of gene expression between different viruses in the remainder of this study.

Viral- and Reporter-Gene Expression in Noncomplementing Cells. Expression analysis by quantitative reverse transcription-PCR (qRT-PCR) of several IE, E, and late (L or γ) genes in infected HDFs confirmed that the ICP0 and ICP27 gene deletions in JΔNI5 reduced viral-gene expression dramatically from the already low levels detected in HDFs infected with JΔNI2 or JΔNI3 at the same gc doses (Fig. S2). Expression of the mCherry reporter gene from its ectopic promoter was also dramatically reduced in JΔNI5-infected HDFs (Fig. S3*A*), ~100-fold by the ICP0 gene deletion (Fig. S3*B*, compare JΔNI2- and JΔNI3-infected

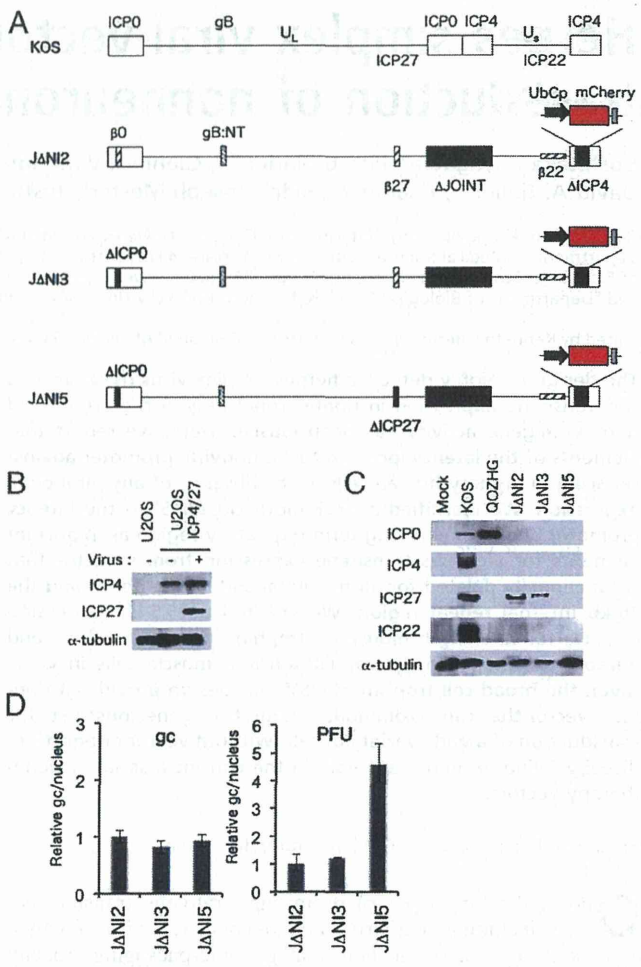

Fig. 1. Vector genome structures and complementing cells for virus production. (*A*) Schematic representations of the genomes of WT HSV-1 KOS, as present in KOS-37 BAC (57), and derivatives JΔNI2, JΔNI3, and JΔNI5. U_L, unique long segment; U_S, unique short segment. The U_S region in KOS-37 BAC and its derivatives is inverted compared with the standard representation of the HSV genome. Open boxes, terminal and internal inverted repeats. Black boxes, deletions (Δ); the ICP47 promoter and translation initiation codon are removed as part of the joint deletion. Cross-hatched horizontal box, the ICP22 IE gene converted to early-expression kinetics by promoter TAATGARAT deletion (β22). All JΔNI recombinants described in this study contain the hyper-activating N/T mutations in the gB gene (gB:NT) (22) and a ubiquitin C promoter (UbCp)-mCherry cassette with the SV40 polyA region in the ICP4 locus. The BAC elements, including a chloramphenicol-resistance gene and β-galactosidase expression cassette, are located between loxP sites in the UL37-UL38 intergenic region (57). (*B*) Western blot analysis of U2OS-ICP4/27 cells. Uninfected cells and cells infected with JΔNI5 virus at an MOI of 1 were harvested at 24 hpi, and extracts were prepared for gel electrophoresis; extracts from uninfected U2OS cells were used as control. Blots were probed with antibodies for ICP4, ICP27, or α-tubulin as a loading control. (*C*) Immunoblot analysis of IE gene products in HDFs. Cells were infected with KOS, QOZHG, or JΔNI viruses at 1 pfu per cell, and extracts were prepared at 24 hpi. Blots were probed with antibodies for the indicated IE gene products or α-tubulin as a loading control. (*D*) Relative nuclear viral DNA levels after infection with equal gc or pfu. HDFs were infected with the indicated JΔNI vectors at 5,000 gc per cell (*Left*) or 1 pfu per cell (*Right*). At 2 hpi, nuclear DNA was isolated, and relative viral gc numbers were determined by qPCR for the gD gene normalized to the cellular 18S rRNA genes.

Table 1. Selected gene modifications in vector constructs

Vector	ICP0	ICP4*	ICP22	ICP27	ICP47	gB[†]	LAT[‡]	UL3/4[§]	UL45/46[§]	UL50/51[§]
KOS	+	+	+	+	+	+	+	—	—	—
KNTc	+	+	+	+	+	N/T	+	UbC-mCherry	—	—
QOZHG	+	Δ	β	CMV-GFP	β	+	+	—	—	—
JΔNI2	β	Δ	β	β	Δp	N/T	3′Δ	—	—	—
JΔNI3	Δ	Δ	β	β	Δp	N/T	3′Δ	—	—	—
JΔNI5	Δ	Δ	β	Δ	Δp	N/T	3′Δ	—	—	—
JΔNI6GFP	Δ	Δ	β	Δ	Δp	N/T	3′Δ	CAG-GFP	—	—
JΔNI7GFP	Δ	Δ	β	Δ	Δp	N/T	CAG-GFP	—	—	—
JΔNI7GFPΔC1	Δ	Δ	β	Δ	Δp	N/T	CAG-GFP, ΔC1	—	—	—
JΔNI7GFPΔC2	Δ	Δ	β	Δ	Δp	N/T	CAG-GFP, ΔC2	—	—	—
JΔNI7GFPΔLP2	Δ	Δ	β	Δ	Δp	N/T	CAG-GFP, ΔLP2	—	—	—
JΔNI7GFPΔC12	Δ	Δ	β	Δ	Δp	N/T	CAG-GFP, ΔC12	—	—	—
JΔNI7GFPΔC12LP2	Δ	Δ	β	Δ	Δp	N/T	CAG-GFP, ΔC12LP2	—	—	—
JΔNI9GW	Δ	Δ	β	Δ	Δp	N/T	Δ	—	GW[¶]	—
JΔNI9GFP	Δ	Δ	β	Δ	Δp	N/T	Δ	—	CAG-GFP	—
JΔNI9LAT-GFP	Δ	Δ	β	Δ	Δp	N/T	Δ	—	LAT-CAG-GFP	—
JΔNI10GW	Δ	Δ	β	Δ	Δp	N/T	Δ	—	—	GW[¶]
JΔNI10GFP	Δ	Δ	β	Δ	Δp	N/T	Δ	—	—	CAG-GFP
JΔNI10LAT-GFP	Δ	Δ	β	Δ	Δp	N/T	Δ	—	—	LAT-CAG-GFP
JΔNI10LAT-GFPΔC12LP2	Δ	Δ	β	Δ	Δp	N/T	Δ	—	—	LATΔC12LP2-CAG-GFP
JΔNI5ΔB#1[#]	Δ	Δ	β	Δ	Δp	N/T	3′Δ	—	—	—
JΔNI5ΔB#2[#]	Δ	Δ	β	Δ	Δp	N/T	3′Δ	—	—	—
JΔNI7GFPΔB[#]	Δ	Δ	β	Δ	Δp	N/T	CAG-GFP	—	—	—
JΔNI7-GWL1	Δ	Δ	β	Δ	Δp	N/T	GW[¶]	—	—	—
JΔNI7mDMDΔB[#]	Δ	Δ	β	Δ	Δp	N/T	CAG-mDMD	—	—	—

+, intact WT gene; β, promoter modifications to change expression kinetics from immediate-early (IE) to early (E); Δ, complete gene deletion; Δp, promoter/start codon deletion. All JΔNI constructs are deleted for the internal repeat (joint) region.
*All JΔNI viruses have the same UbC promoter-mCherry expression cassette in the deleted ICP4 locus.
[†]N/T, gB:D285N/A549T allele referred to herein as gB:N/T.
[‡]3′Δ, deletion in the LAT primary transcript region resulting from deletion of the ICP0 promoter and coding region (GenBank JQ673480, positions 1,522–5,500) or promoter alone (JΔNI2, GenBank positions 1,522–2,234). Replacement insertions within the remaining portion of the LAT 2-kb intron are specified.
[§]Insertions are specified; —, no insertion.
[¶]GW, gateway recombination cassette.
[#]BAC-deleted viruses.

cells) and another approximately eightfold by the additional deletion of the ICP27 gene (JΔNI3- vs. JΔNI5-infected cells). These observations confirmed that the residual ICP0 and ICP27 expression from JΔNI2 is sufficient to prevent global transcriptional silencing of the viral genome whereas deletion of these two genes essentially eliminated all native and exogenous promoter activity. Consistent with published studies (13), mCherry expression could be induced in JΔNI5-infected HDFs by superinfection with a replication-defective ICP0$^+$ virus [QOZHG; ICP4$^-$/ICP27$^-$/β-ICP22/β-ICP47 (23)] (Fig. S3*C*). Thus, ICP27 was not required to derepress the silent JΔNI5 genome, and the small amount of ICP0 expressed in JΔNI2-infected HDFs was sufficient to support limited transcriptional activity throughout the viral genome.

The LAT Locus Supports High-Level Transgene Expression from the Silent JΔNI5 Genome. Upon infection of neuronal cells, HSV enters a latent state in which the viral genome is transcriptionally silent except for the LAT locus. We explored whether the LAT locus would similarly allow a cellular promoter to remain active in nonneuronal cells in the context of an otherwise silent viral genome. To this end, we introduced an expression cassette consisting of the CAG enhancer/promoter and EGFP gene (CAGp-GFP) into the LAT 2-kb intron region of JΔNI5, creating a vector construct referred to as JΔNI7GFP (Fig. 2*A*). As a control, we introduced the same CAGp-GFP cassette into the UL3-UL4 intergenic region of JΔNI5, producing vector JΔNI6GFP (Fig. 2*A*); the UL3-UL4 intergenic region has been used by others for nondisruptive insertion of transgene cassettes (24, 25) and is close to, but outside, the LAT locus. Infectious viruses were produced on U2OS-ICP4/27 cells, and the gc:PFU ratios of the new virus

Table 2. Virus titers

Virus	gc/mL (× 10^{11})	pfu/mL (× 10^8)	gc/pfu
KOS	5.33	130.00	41.02
KNTc	8.15	29.60	275.23
QOZHG	1.55	2.33	663.54
JΔNI2	3.28	4.00	819.98
JΔNI3	3.46	3.36	1,028.43
JΔNI5	11.74	5.00	2,347.65
JΔNI6GFP	7.30	2.66	2,744.20
JΔNI7GFP	3.99	1.86	2,144.88
JΔNI7GFPΔC1	1.66	0.50	3,310.18
JΔNI7GFPΔC2	8.42	3.50	2,405.25
JΔNI7GFPΔLP2	4.75	1.70	2,796.75
JΔNI7GFPΔC12	5.97	1.86	3,211.54
JΔNI7GFPΔC12LP2	8.03	3.00	2,676.55
JΔNI9GFP	6.70	2.00	3,352.08
JΔNI9LAT-GFP	5.58	2.66	2,097.43
JΔNI10GFP	10.50	1.66	6,328.27
JΔNI10LAT-GFP	2.30	0.93	2,460.11
JΔNI10LAT-GFPΔC12LP2	2.69	1.23	2,186.17
JΔNI5ΔB#1	6.50	8.66	750.98
JΔNI5ΔB#2	10.18	14.60	697.53
JΔNI7GFPΔB	26.55	14.30	1,856.67
JΔNI7mDMDΔB	7.01	3.66	1,916.53

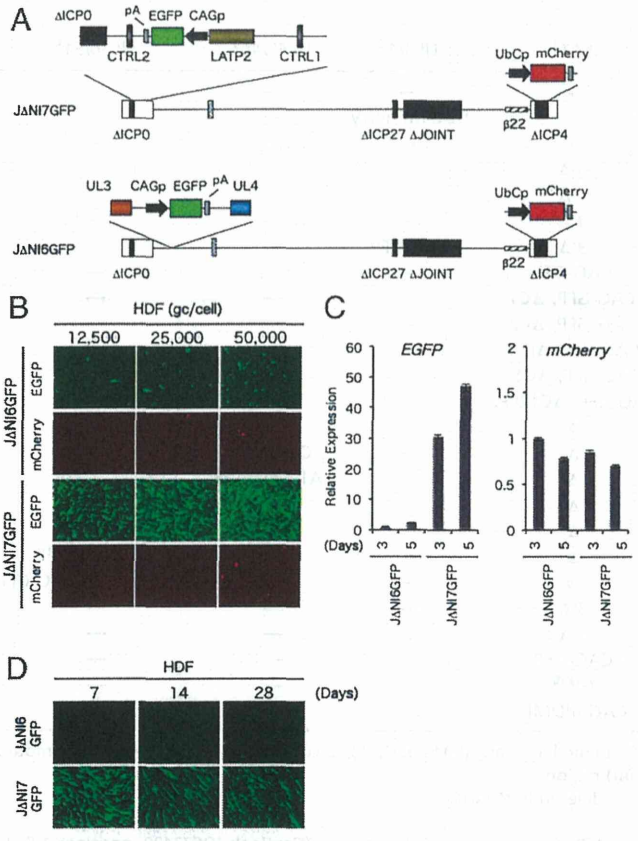

Fig. 2. JΔNI6GFP and JΔNI7GFP genome structures and reporter-gene expression. (*A*) JΔNI7GFP contains a CAG promoter-EGFP expression cassette with the rabbit β-globin polyA (pA) region in the 2-kb LAT intron region between the LATP2 long-term expression/enhancer region and a downstream series of CTCF-binding motifs (CTRL2) in the intron. LATP2 extends from the LAT transcription initiation site to within the 2-kb intron. JΔNI6GFP contains the same CAG promoter-EGFP expression cassette between the UL3 and UL4 genes. (*B–D*) EGFP and mCherry expression in infected HDFs. (*B*) Cells were infected with JΔNI6GFP or JΔNI7GFP virus at different gc per cell, and fluorescence was visualized at 3 dpi. (*C*) HDFs were infected with JΔNI6GFP or JΔNI7GFP vector at 12,500 gc per cell and harvested 3 or 5 d later for mRNA extraction and qRT-PCR analysis for the two reporter genes. Expression normalized to 18S rRNA is shown relative to JΔNI6GFP-infected cells on day 3. (*D*) HDFs were infected with JΔNI6GFP or JΔNI7GFP virus at 25,000 gc per cell, and EGFP fluorescence was photographed at 7, 14, and 28 dpi.

stocks were similar to that of JΔNI5 (Table 2). Both JΔNI6GFP and JΔNI7GFP produced abundant green and red fluorescence during amplification in U2OS-ICP4/27 cells, confirming the integrity of their transgene-expression cassettes. To examine the abilities of these viruses to express the EGFP transgene in noncomplementing cells, HDFs were infected with increasing gc per cell, and EGFP fluorescence was recorded at 3 dpi (Fig. 2*B*). JΔNI7GFP-infected cells showed abundant, viral dose-dependent EGFP expression whereas JΔNI6GFP infection produced limited expression, even at the highest dose. Although we used a higher virus input here than in earlier JΔNI5 infections, mCherry expression remained minimal. These results were confirmed by qRT-PCR measurements of EGFP and mCherry mRNA levels at 3 and 5 dpi (Fig. 2*C*) and were consistent with the suggestion that the JΔNI6GFP and JΔNI7GFP virus genomes, like the JΔNI5 genome, were silent in infected HDFs whereas the LAT locus maintained transcriptional activity from a non-HSV promoter. Because EGFP mRNA levels in JΔNI7GFP-infected cells were at least as high at 5 dpi as at 3 dpi (Fig. 2*C*), we asked whether expression could be detected at later times when the cells are fully contact-inhibited. The results showed that expression could persist for at least 4 wk in some of the cells (Fig. 2*D*). Together, these observations indicated that the LAT locus is a privileged site for durable transgene expression in nonneuronal cells in the background of an HSV genome that lacks all IE gene expression.

CTRLs and LATP2 Support Transgene Expression from the LAT Locus. It has been demonstrated that LAT expression during latency is controlled by the latency-associated promoters (LAPs) 1 and 2 (26, 27). LAP1 is located upstream of the transcription initiation site of the ~8.3-kb unstable primary LAT transcript that is processed to a stable 2-kb LAT intron whereas LAP2 is located downstream of LAP1 in the first exon and extending into the 2-kb intron region. A LAP2-containing region extending somewhat further into the intron has been referred to as LATP2 (8). In addition to acting as a promoter, it has been shown that the LAP2/LATP2 region can act as a position-independent long-term expression/enhancer element for transgene expression in neurons (8, 28). However, it has also been reported that the LAT locus is protected from global silencing of the viral genome during latency by regions rich in CTCF-binding sites, termed CTRLs, one located upstream of LAP1 (CTRL1) and the other in the 2-kb intron just downstream of LATP2 (CTRL2) (29). We therefore explored the potential roles of the LATP2 and CTRL elements in enabling the observed EGFP expression in JΔNI7GFP-infected HDFs. We deleted the three elements separately and in combination from the JΔNI7GFP genome (Fig. 3*A*) and examined reporter-gene expression in infected HDFs (Fig. 3 *B* and *C*). Deletion of either CTRL1 (ΔC1) or LATP2 (ΔLP2) caused a marked decrease in green fluorescence and EGFP mRNA levels whereas the deletion of CTRL2 (ΔC2) had only a minor effect. Deletion of both CTRLs (ΔC12) had the same effect as the deletion of CTRL1 alone whereas deletion of all three elements (ΔC12LP2) reduced expression further to the level observed in JΔNI6GFP-infected cells. As expected, mCherry fluorescence was visually undetectable in any of the infected cells (Fig. 3*B*), suggesting that the different deletions did not cause derepression of other sites in the viral genome. These results indicated that both CTRL1 and the LATP2 region play significant roles in protecting the linked transgene from transcriptional silencing in the context of a viral genome that is functionally devoid of all IE genes.

LAT Locus Protection of Transgene Expression Is Position-Independent. To determine whether sequences associated with the LAT locus are sufficient to protect an embedded transgene expression cassette against silencing in the absence of IE gene products, we inserted a restriction fragment corresponding to the LAT:CAGp-GFP region of JΔNI7GFP, including the two CTRLs, LAP1 and LATP2, at one of two ectopic positions in a JΔNI5 derivative that was deleted for the same LAT region to avoid recombination between the native and new sites. We first engineered a Gateway (GW) recombination cassette into the intergenic region between UL45 and UL46 (JΔNI9GW) or between UL50 and UL51 (JΔNI10GW) of the LAT-deleted JΔNI5 genome (JΔNI5ΔL) (*SI Materials and Methods*) and then introduced the LAT:CAGp-GFP fragment or just CAGp-GFP without LAT sequences by recombination with the GW cassette (Fig. 4*A*). After virus production on U2OS-ICP4/27 cells (Table 2), the vectors were tested for reporter-gene expression in infected HDFs. At 3 dpi, the vectors that lacked LAT sequences surrounding the reporter cassette (JΔNI9GFP and JΔNI10GFP) showed low levels of EGFP fluorescence (Fig. 4*B*) and mRNA (Fig. 4*C*) in infected cells, similar to the JΔNI6GFP control vector, suggesting that the two intergenic insertion sites were transcriptionally repressed, like the intergenic region between UL3 and UL4 (Fig. 2). However,

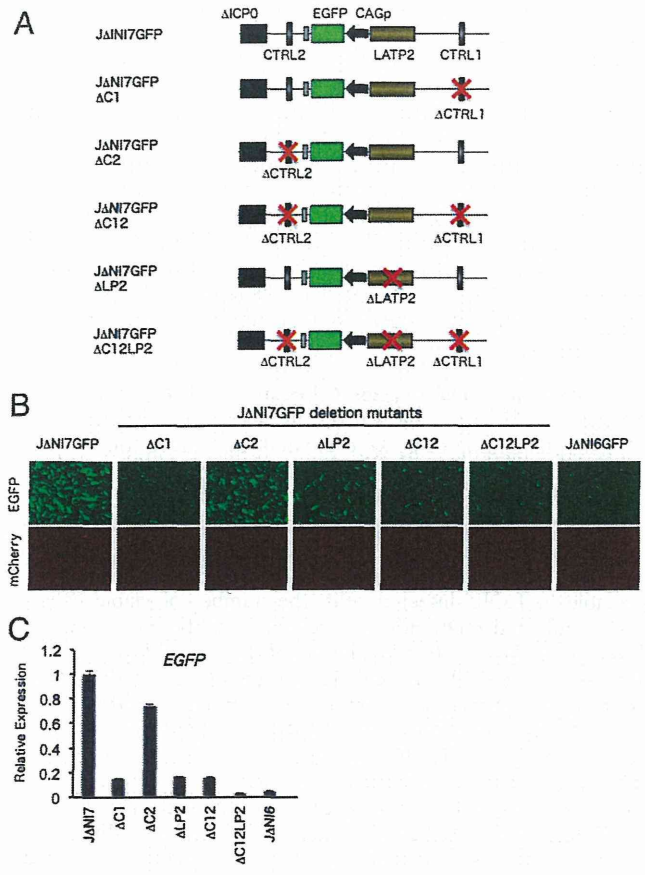

Fig. 3. Effect of LAT locus elements on EGFP expression from JΔNI7GFP. (*A*) Genome representations of JΔNI7GFP and derivatives deleted for CTRL1 (ΔC1), CTRL2 (ΔC2), or LATP2 (ΔLP2) individually or in combinations. (*B*) Reporter-gene expression in infected HDFs. Cells were infected with the indicated viruses at 12,500 gc per cell, and fluorescence was recorded at 3 dpi. (*C*) Relative EGFP mRNA levels in HDFs infected with JΔNI7GFP, derivatives deleted for LAT elements, or JΔNI6GFP; viruses are identified by abbreviated names. Cells were infected at 12,500 gc per cell and processed at 3 dpi for qRT-PCR analysis. Expression levels were normalized to 18S rRNA and are presented relative to the level in JΔNI7GFP-infected cells.

when the reporter cassette was flanked at both sides by LAT sequences (vectors JΔNI9LAT-GFP and JΔNI10LAT-GFP), EGFP expression increased to the level observed in JΔNI7GFP-infected cells (Fig. 4*B*), indicating that the antisilencing activity of the LAT-derived regions is functional in a position-independent manner. To confirm the dependence of this activity on LATP2 and either or both CTRLs, we introduced a LATP2- and CTRL-deleted version of the LAT:CAGp-GFP fragment by GW recombination into the JΔNI10GW genome; the deletions were the same as those in the LAT region of the earlier JΔNI7GFPΔC12LP2 vector (Fig. 3*A*). We found that the deletions reduced EGFP expression in infected HDFs, although not fully down to the level observed with the LAT-free JΔNI10GFP vector (Fig. 4 *C* and *D*); it is unclear why the ΔC12LP2 deletions seemed to have a smaller effect here (~3.5-fold) than in JΔNI7GFP (~50-fold) (Fig. 3*C*). However, our results clearly demonstrate that a portion of the LAT locus that includes the two CTRLs, LAP1 and LATP2, can protect an embedded transgene expression cassette in a position-independent manner against global silencing of the viral genome in the absence of IE gene expression and indicate that at least CTRL1 and LATP2 play a role in this activity. We also determined whether the effect of the transferred LAT sequences was limited to the embedded transgene. We observed moderate increases in the levels of ICP22, ICP6, and glycoprotein C (gC) mRNA produced by JΔNI10LAT-GFP compared with JΔNI10GFP (Fig. S4), but these increases were substantially smaller than the increase in GFP expression (Fig. 4*B*). Of interest, expression of the three distal genes was also somewhat higher from JΔNI10LAT-GFP than from JΔNI5 (Fig. S4), suggesting that the reach of the LAT elements may be influenced by their context.

LAT Locus Elements Protect Transgene Expression in Other Cell Types. To evaluate the applicability of our observations beyond HDFs,

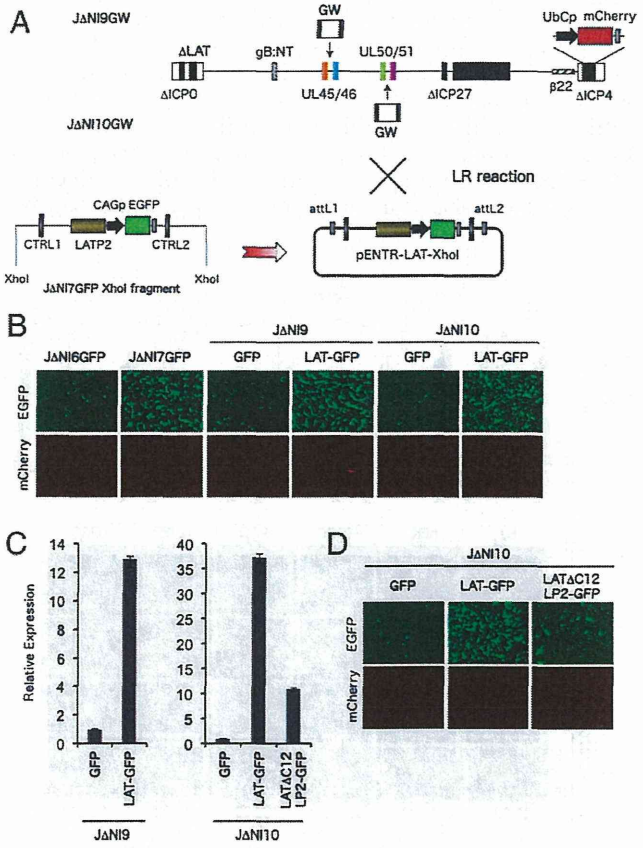

Fig. 4. Anti-silencing activity of LAT sequences positioned elsewhere in the viral genome. (*A*) Construction of JΔNI9 and JΔNI10 vectors. A LAT region spanning CTRL1, LATP2, and CTRL2 was removed from the JΔNI5 genome (ΔLAT), and a GW recombination cassette was introduced between UL45 and UL46 to generate JΔNI9GW or between UL50 and UL51 to produce JΔNI10GW (*Upper*). XhoI restriction sites were used to isolate a CAGp-GFP–containing LAT fragment from JΔNI7GFP (*Lower Left*). The XhoI fragment was cloned into pENTR1A (*Lower Right*) and transferred into JΔNI9GW or JΔNI10GW by *attL*/*attR* recombination with the respective GW cassettes (LR reaction) to produce JΔNI9LAT-GFP and JΔNI10LAT-GFP, respectively. As controls, we also recombined the CAGp-GFP cassette without LAT sequences via a pENTR1A intermediate into the GW locus of JΔNI9GW or JΔNI10GW, producing JΔNI9GFP and JΔNI10GFP. (*B*) Reporter-gene expression in HDFs infected with JΔNI9 or JΔNI10 viruses. HDFs were infected with the indicated viruses at 12,500 gc per cell. EGFP and mCherry fluorescence were recorded at 3 dpi. (*C*) EGFP mRNA levels in infected HDFs determined by qRT-PCR as in earlier figures. Levels are shown relative to JΔNI9GFP- or JΔNI10GFP-infected cells. JΔNI10ΔC12LP2-GFP was constructed by transfer of the XhoI LAT fragment from JΔNI7ΔC12LP2-GFP into the GW site of JΔNI10GW, similar to the construction of JΔNI10LAT-GFP above. (*D*) Effect of the deletion of both CTRLs and LATP2 from JΔNI10LAT-GFP on transgene expression. HDFs were infected at 12,500 gc per cell, and EGFP and mCherry fluorescence were recorded at 3 dpi.

we tested EGFP and mCherry expression from selected vectors in other cell types. By qRT-PCR, we observed higher EGFP mRNA levels in JΔNI7GFP-infected than in JΔNI6GFP-infected human cells at 3 dpi (Fig. 5*A*). The greatest difference was observed in BJ human foreskin fibroblasts (~35-fold), similar to the difference in HDFs (~30-fold) (Fig. 2*C*). Human neonatal keratinocytes (hEKs) showed the smallest difference (~4.5-fold), with intermediate values seen in human muscle-derived stem cells (hMDSCs) (~10-fold), human preadipocytes (hPADs) (approximately sevenfold), and human hepatocytes (hHEPs) (~13-fold). We also compared the two vectors in fetal rat dorsal root ganglion (rDRG) neurons and found only a ~2.5-fold difference. Fig. 5*B* shows representative fluorescence images at 3 dpi from an independent experiment performed under the same infection conditions. The results were largely consistent with the qRT-PCR data. Of interest, whereas none of the human cells showed significant mCherry fluorescence, abundant mCherry expression was observed in both the JΔNI6GFP- and JΔNI7GFP-infected rat DRG cultures. It is not yet known whether this observation is unique to neuronal cells and may be a function of the promoter driving mCherry-gene expression, the location of the expression cassette in the viral genome, and/or the rat origin of the cells. We

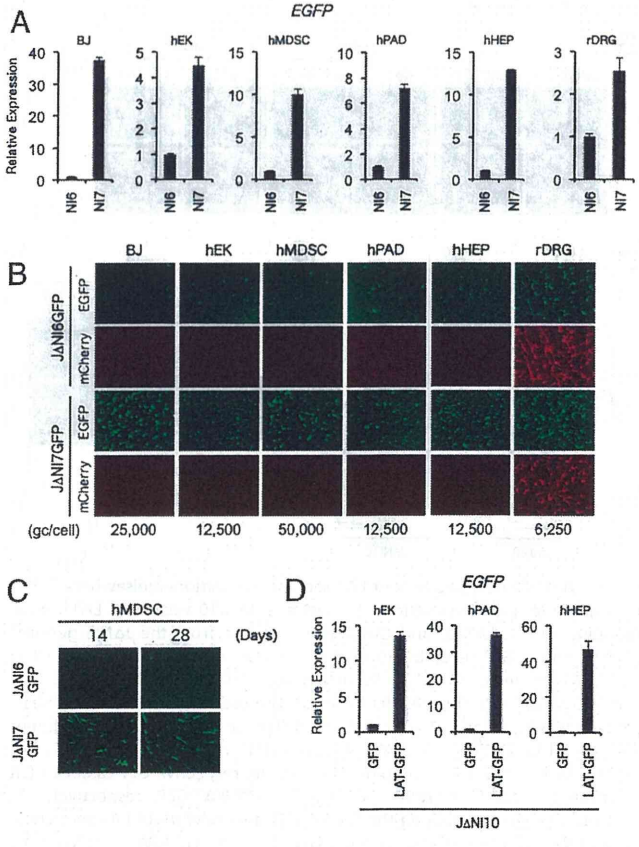

Fig. 5. Reporter-gene expression from JΔNI vectors in other noncomplementing cells. (*A*) The cells listed at the top were infected with JΔNI6GFP or JΔNI7GFP at the gc per cell indicated below the panels of *B*. EGFP and mCherry fluorescence were recorded at 3 dpi. (*B*) EGFP gene expression in cells infected as in *A* was measured at 3 dpi by qRT-PCR analysis. Results normalized to 18S rRNA are shown relative to JΔNI6GFP-infected cells. (*C*) hMDSCs were infected with JΔNI6GFP or JΔNI7GFP virus at 50,000 gc per cell, and EGFP fluorescence was photographed at 14 and 28 dpi. (*D*) qRT-PCR determination of EGFP mRNA levels in hEK, hPAD, and hHEP cells 3 d after infection with JΔNI10GFP or JΔNI10LAT-GFP at 12,500 gc per cell. Normalized expression is shown relative to JΔNI10GFP-infected cells.

were able to maintain hMDSCs for an extended period, allowing the monitoring of EGFP expression over time in JΔNI7GFP-infected cells. As shown in Fig. 5*C*, EGFP remained detectable for at least 4 wk after infection, similar to our observation with JΔNI7GFP-infected HDFs (Fig. 2*D*). Lastly, we determined for some of the cells whether CAGp-GFP activity in the UL50/51 intergenic region was enhanced by flanking LAT sequences as in HDFs. The results in Fig. 5*D* show a substantial enhancement in all three cell types that may, for unknown reasons, exceed the difference between JΔNI6GFP and JΔNI7GFP in the same cells. Overall, these results indicated that the position-independent antisilencing activity of genetic elements in the LAT locus is not limited to HDFs but is operative in a variety of nonneuronal human cell types.

Elimination of Residual Vector Cytotoxicity by BAC Removal. Although JΔNI5 and its derivatives displayed no overt toxicity for noncomplementing cells, we evaluated this perception by quantitative cell viability (MTT) assay. HDFs and Vero cells were infected with KOS, QOZHG, JΔNI2, JΔNI3, or JΔNI5 virus at 25,000 gc per cell, and assays were performed at 5 dpi. Surprisingly, whereas toxicity for Vero cells was significantly reduced between JΔNI2 and JΔNI3 ($P < 0.001$) and was no longer detectable in JΔNI5-infected cells, the number of viable cells in JΔNI5-infected HDF cultures remained well below the number in mock-infected cultures and was not dramatically greater than that in JΔNI2- or JΔNI3-infected cultures (Fig. 6*A*); QOZHG, which overexpresses ICP0, was highly toxic for HDFs, similar to replication-competent virus (KOS). A significant difference between JΔNI5 and a fully IE gene-inactivated vector such as *d*109 that was previously shown to be devoid of any toxicity for human fibroblasts (13) is the presence of the loxP-flanked 11-kb BAC region in the JΔNI5 genome. To eliminate this region from our vectors, we used retroviral transduction to produce a JΔNI5-complementing cell line expressing Cre recombinase, U2OS-ICP4/27-Cre cells (Fig. S5*A* and *SI Materials and Methods*). After infection of these cells with JΔNI5 virus, plaques were screened by staining for LacZ activity expressed from the BAC cassette, two negative viral clones were purified (JΔNI5ΔB#1 and JΔNI5ΔB#2), and accurate excision of the BAC region was confirmed by PCR and sequencing through the remaining loxP site (*SI Materials and Methods*). Cell-viability assays showed unimpaired growth of JΔNI5ΔB-infected HDFs compared with mock-infected HDFs whereas the BAC-positive JΔNI5 virus again inhibited HDF growth (Fig. 6*B*). We next determined whether the BAC region affects short- and long-term transgene expression. We generated a BAC-deleted version of JΔNI7GFP (JΔNI7GFPΔB) (Fig. S5*B*) and recorded EGFP expression over time in infected HDFs compared with infections with BAC-positive JΔNI6GFP and JΔNI7GFP (Fig. 6*C*); cytosine arabinoside (AraC) was included in the postinfection maintenance media in this experiment to block cell division to prevent dilution of vector genomes. No dramatic differences were observed in EGFP fluorescence levels between JΔNI7GFPΔB- and JΔNI7GFP-infected cells through 28 d postinfection. In the same experiment, qRT-PCR measurements showed a moderately slower decline in EGFP gene expression in JΔNI7GFPΔB- than in JΔNI7GFP-infected HDFs (Fig. 6*D*). Together, these results indicated that BAC deletion is advantageous for sustained transgene expression in nondividing cells whereas the opposite effect may be observed in dividing cells in vitro due to a higher rate of cell division and thus faster dilution of viral genomes.

Efficient Transduction of Dystrophin with the JΔNI5 System. To illustrate the capacity of the JΔNI5 vector system, we chose to insert the complete 14-kb cDNA encoding the murine version of dystrophin, the defective protein in Duchenne muscular dystrophy (DMD) (30). Currently no helper-independent viral-vector

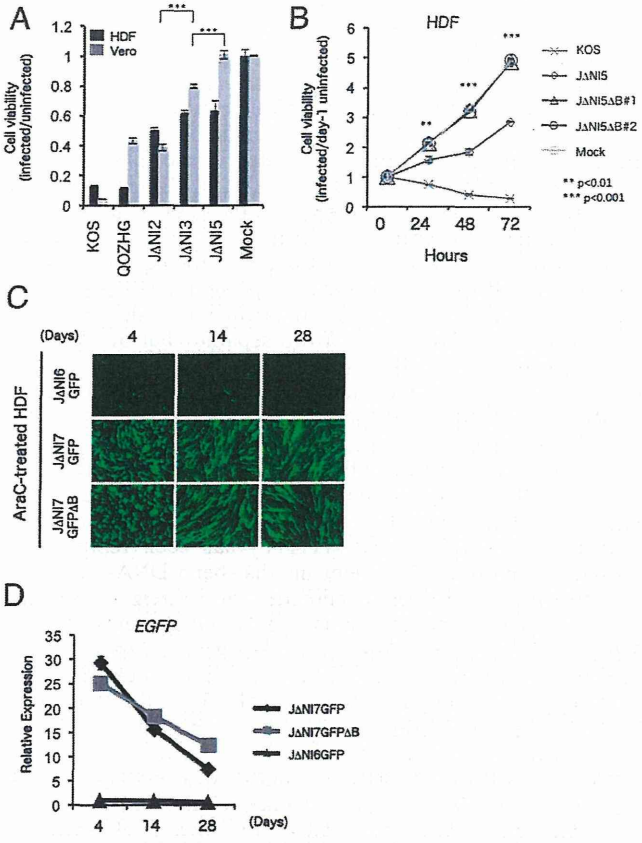

Fig. 6. Residual JΔNI5 cytotoxicity and effects of BAC excision. (*A*) In vitro cytotoxicity assay. HDFs and Vero cells were infected at 25,000 gc per cell, and cell viability in triplicate wells was measured at 5 dpi by MTT assay. Plotted values represent the mean ratios of virus-infected to mock-infected cells. Differences between JΔNI2- and JΔNI3-infected Vero cells and between JΔNI3- and JΔNI5-infected Vero cells (brackets) were statistically highly significant (***$P < 0.001$). (*B*) BAC deletion eliminates JΔNI5 vector toxicity for HDFs. HDFs (2×10^3) were infected with KOS, JΔNI5, or two different JΔNI5ΔB isolates at 25,000 gc per cell, and cell viability in triplicate wells was measured by MTT assay at the indicated hpi. Plotted values represent the mean ratios of virus-infected to day-1 mock-infected cells. Statistically significant differences between JΔNI5-infected and both JΔNI5ΔB#1- and JΔNI5ΔB#2-infected cells are indicated by asterisks (**$P < 0.01$; ***$P < 0.001$). (*C*) Effect of BAC excision on JΔNI7GFP reporter-gene expression. HDFs were infected with JΔNI6GFP, JΔNI7GFP, or BAC-deleted JΔNI7GFP (JΔNI7GFPΔB) at 25,000 gc per cell, and EGFP fluorescence was visualized at 4, 14, and 28 dpi. To prevent vector dilution by cell division, 1 μM AraC (Sigma) was included in the postinfection maintenance media. (*D*) EGFP mRNA levels in cells infected with JΔNI6GFP, JΔNI7GFP, or JΔNI7GFPΔB viruses. HDFs were infected at 25,000 gc per cell and harvested on the indicated days postinfection for mRNA extraction and qRT-PCR quantification of EGFP gene expression. Data were normalized to viral gc numbers determined in the same cultures and is presented relative to the normalized value of JΔNI6GFP-infected cells on day 4.

system exists that is capable of vigorous production of full-length murine or human dystrophin. We modified the JΔNI5 genome by insertion of a GW cassette into the LAT region between LATP2 and CTRL2, creating JΔNI7-GWL1, and then recombined the cassette with the 16.5-kb insert of a pENTR construct containing the complete mouse dystrophin cDNA between the CAG promoter and the rabbit β-globin polyadenylation region (Fig. S6). Including the mCherry expression cassette, the resulting vector construct, JΔNI7-mDMD, carried ~20 kb of transgene sequences in addition to the BAC region. A small virus stock was generated by transfection of U2OS-ICP4/27 cells, the BAC region was deleted as described above by passage through U2OS-ICP4/27-Cre cells, and a clonal isolate referred to as JΔNI7-mDMDΔB was amplified to high titer (Table 2). Dystrophin-deficient *mdx* mouse-derived muscle progenitor cells infected with JΔNI7-mDMDΔB showed the presence of full-length dystrophin at 3 dpi (Fig. 7*A*) and wide-spread expression in differentiated cultures at 7 dpi (Fig. 7*B*), supporting the utility of the JΔNI5 vector backbone for efficient transduction of nonneuronal cells with large genes that cannot be accommodated by current vector systems.

Discussion

HSV offers a number of important features as a gene-therapy vector, including its ability to infect a wide range of cells and establish the viral genome as a stable extrachromosomal element, efficient low-dose transduction that helps reduce inflammation and the induction of antiviral immunity, and a very large payload capacity that easily exceeds that of most vectors in current use. However, whereas delivery of large payloads represents an important unmet need in the gene-therapy field, it has not been possible to create HSV vectors that provide robust and persistent transgene expression in the absence of cytotoxic viral IE gene expression.

Our study reports the engineering of HSV vectors that are both noncytotoxic and capable of persistent transgene expression. We created an HSV backbone that does not produce any IE proteins in noncomplementing cells and explored the possibility that the latency locus could be exploited to protect an embedded cellular promoter against global silencing of the viral

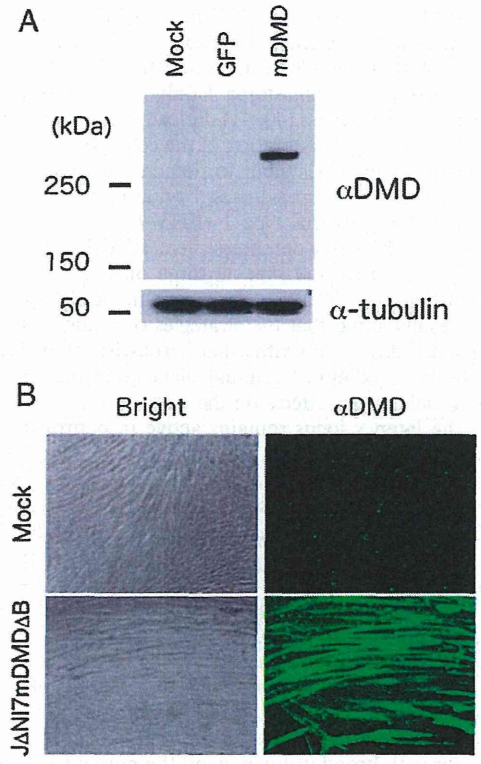

Fig. 7. Efficient JΔNI-mediated transduction by a large transgene. (*A*) Western blot analysis of dystrophin expression in mock-, JΔNI7GFPΔB-, and JΔNI7mDMDΔB-infected *mdx* mouse-derived muscle progenitor cells (25,000 gc per cell) at 3 dpi. (*Upper*) Anti-dystrophin antibody (αDMD). (*Lower*) Anti–α-tubulin antibody (α-tubulin) as loading control. (*B*) Dystrophin immunofluorescence (αDMD) and bright-field (Bright) images of mock- and JΔNI7mDMDΔB-infected *mdx* muscle progenitor cells (50,000 gc per cell) at 7 dpi.